Extreme ^{17,18}O-rich materials from the Acfer 094 carbonaceous chondrite

By
Naoya Sakamoto

Department of Natural History Sciences
Graduate School of Science
Hokkaido University

Doctor Thesis
2007

ABSTRACT

This thesis reports an in situ discovery of a chemically and isotopically unique material distributed ubiquitously in fine-grained matrix of a primitive carbonaceous chondrite Acfer 094. Oxygen isotopic composition of our Solar System is believed to have resulted from mixing of two isotopically distinct nebular reservoirs, ^{16}O-rich and ^{17,18}O-rich relative to Earth. Although ^{16}O-rich reservoir is suggested as high temperature condensations in the solar nebula by the studies of refractory inclusions in meteorites, the nature and composition of the ^{17,18}O-rich reservoir are poorly understood. The purpose of this thesis is to constrain the ^{17,18}O-rich reservoir and clarify the origin of oxygen isotopic heterogeneity in the solar system.

In chapter 2, analytical methods and conditions of this thesis are described in detail. A polished thin section of Acfer 094 ungrouped carbonaceous chondrite shows no evidence for aqueous alteration and thermal metamorphism and Murchison CM2 chondrite shows heavy aqueous alteration were prepared. A field-emission type scanning electron microprobe and an analytical transmission electron microscope have used for petrologic study, and isotope microscope composed of direct combination of secondary ion mass spectrometry and 2-dimentional ion detector has used for isotopic study.

In chapter 3, the results of petrologic, isotopic and thermodynamic analysis have described. The isotopically anomalous materials (referred as "new-PCP" in this thesis) have discovered from Acfer 094 by isotopic study. The material is mainly composed of iron, oxygen, and sulfur, and is highly enriched in ^{17}O and ^{18}O (up to +180‰) relative to Earth's ocean. The chemical compositions of new-PCP are homogeneous and mainly composed of Fe, Ni, O and S (representatively in weight percent wt%, Fe, 61.6; Ni, 5.4; O, 19.3; S, 9.6; Mg, 0.1; Si, 0.2). Mineralogical observations reveal the fractured troilite are often attached to new-PCP and consist of aggregates of nanocrystals with a size range of 10-200 nm. The electron diffraction patterns from ~100-nm-sized individual crystals show that the main spots of the crystals are similar to those of magnetite. In addition, there are weak extra spots suggesting a 3-fold superstructure. Based on the unique chemical composition of new-PCP, we have counted the new-PCP grains in an Acfer 094 thin section. The new-PCP grains are ubiquitous and scattered randomly throughout the Acfer 094 matrix. Twenty-two new-PCPs (the largest is 160 μm^2) were identified in 11mm^2 area of the matrix. This corresponds to 94±20 (σ) parts per million (ppm) by volume. In order to compare with

new-PCP, serpentine-tochilinite intergrowths (previously called ''poorly characterized phases'' or PCP) from Murchison has also analyzed. Although the element species in the new-PCP are also main components of tochilinite, the O/S atom ratios of new-PCP are about 4 times larger than in tochilinite and the oxygen isotopic composition of tochilinite was similar to the matrix supporting the aqueous alteration formation on the parent body. Thermodynamic calculation shows the Fe-O-S-bearing material would form below 360K in the typical solar nebula.

In chapter 4, the formation environment and the origin of new-PCP have discussed. Mineralogical observations and thermodynamic analysis suggest that this material resulted from oxidation of iron-metal and/or iron-sulfide by water in the solar nebula or on a planetesimal. The new-PCP would be formed inside the water sublimation front (snowline) of the solar nebula because water vapor is the major oxidant in the solar nebula and the sublimation temperature of water ice is below 200K even in the several-fold H_2O-enriched nebula. The extremely heavy oxygen isotopic composition of the new-PCP argues against the formation by aqueous alteration mechanism on the parent body because the oxygen isotopic compositions of new-PCP plot away from the aqueous alteration fractionation line which is considered to be a reaction path between aqueous solution and matrix silicates toward the isotope equilibrium. Therefore, the conventional aqueous alteration models are excluded for the formation process of new-PCP. The lack of mineralogical and petrographical evidence of aqueous alteration of Acfer 094 also support the non-conventional alteration model. If the new-PCP were formed in a planetesimal setting, a plausible oxidant would be water vapor or aqueous solution that originated from accreted nebular ice and did not experience oxygen isotope exchange with the matrix silicates. In either case, the oxygen isotopic composition of nebula water would be preserved in the new-PCP that is the new ^{17,18}O-rich end-member ($\delta^{17,18}O_{SMOW}$= +180‰) of the Solar System. Therefore, the oxygen isotopic composition of the new-PCP must represent composition of the nebular water and the previously hypothesized ^{17}O- and ^{18}O-rich reservoir in the early Solar System

In chapter5 is a conclusion of this thesis. Oxygen isotopic composition of new-PCP shows highly enriched in ^{17}O and ^{18}O ($\delta^{17,18}O_{SMOW}$ = +180‰), providing the first evidence for an extremely ^{17,18}O-rich reservoir in the early Solar System. The oxygen isotopic heterogeneity in our solar system has expanded more than three times larger ever thought. The extreme oxygen isotopic composition of new-PCP was inferred to be recorded composition of this primordial water, that corresponds to an ^{17,18}O-rich nebular reservoir in the early Solar System, in agreement with the self-shielding models.

CONTENTS

1. INTRODUCTION

1.1. Oxygen Isotopes in Meteorites

Oxygen is the third most abundant element in the Solar System and the most abundant element of the terrestrial planets. The presence of oxygen in both gaseous and solid phases makes oxygen isotopes (^{16}O, ^{17}O, ^{18}O) important tracers of various fractionation processes in the solar nebula, which are essential for understanding the evolution of gaseous and solid phases in the early Solar System. Therefore, the drastic change of the formation scenario for our Solar System could be inspired by the discovery of unexplained oxygen isotope heterogeneity from meteorites in 1973 (Clayton et al., 1973). This problem is still remained one of the biggest challenges in the cosmochemistry.

Oxygen isotopes are formed in different nucleosynthetic processes, so that stellar nucleosynthesis can produce isotopic heterogeneity. The abundant isotope, ^{16}O (99.76% in Earth's ocean), is produced in stellar nucleosyntheis by helium burning. The rare isotopes, ^{17}O (0.04%) and ^{18}O (0.20%), are produced by hot CNO cycles in zones rich in H and He, respectively, in both novae and super novae. For all three isotopes, rapid cooling of stellar ejecta can lead to the formation of molecules and/or refractory solids, which bear the signature of the particular nucleosynthetic processes. Therefore, the interstellar medium should contain molecules and grains that have anomalous abundances of the isotopes of oxygen and of the elements with which it is combined. These molecules and particles are preserved in primitive meteorites and observed with a wide range of isotopic compositions as presolar grains.

Oxygen isotopic compositions are normally expressed in δ units, which are deviations in part per thousand (permil, ‰) in the $^{17}O/^{16}O$ and $^{18}O/^{16}O$ ratios from terrestrial Standard Mean Ocean Water (SMOW): $\delta^{17,18}O_{SMOW} = [(^{17,18}O/^{16}O)_{sample}/(^{17,18}O/^{16}O)_{SMOW} - 1] \times 1000$. The oxygen isotopic anomalies well distinguished with a three-isotope diagram $\delta^{18}O$ vs. $\delta^{17}O$ (Figure 1). The isotopic fractionation resulting from a normal chemical process, depends on the mass differences among isotopes: the fractionation takes place along a line with a slope of 1/2 on the oxygen three-isotope diagram, or the fraction of ^{18}O relative to ^{16}O occurs twice as much compared with the fractionation of ^{17}O relative to ^{16}O. On a three-isotope diagram of $\delta^{18}O$ vs. $\delta^{17}O$, compositions of nearly all terrestrial samples and Moon samples plot along a single line of slope 0.52 called the terrestrial fractionation (TF) line. The O isotope ratios ($^{18}O/^{16}O$ and $^{17}O/^{16}O$) of CAI minerals observed in carbonaceous

chondrites by Clayton et al (1973), on the other hand, distributed along a line called carbonaceous chondrite anhydrous minerals (CCAM) line having a slope of unity, instead of 1/2 generally observed for natural terrestrial and laboratory samples. Carbonaceous chondrites were believed as the most primitive meteorites within any meteorites because chondrite consists of undifferentiated constituents, with the various proportions of refractory inclusions, chondrules, matrix and metal. The O-isotopic compositions of the vast majority of extraterrestrial samples, including chondrites, achondrites, cometary dust, and Martian meteorites, deviate from the terrestrial fractionation line, reflecting mass-independent fractionation processes. On this diagram, oxygen isotopic compositions of primitive chondrite components (chondrules, refractory inclusions, and fine-grained matrix) define a line with a slope of ~1 (Young and Russell, 1998).

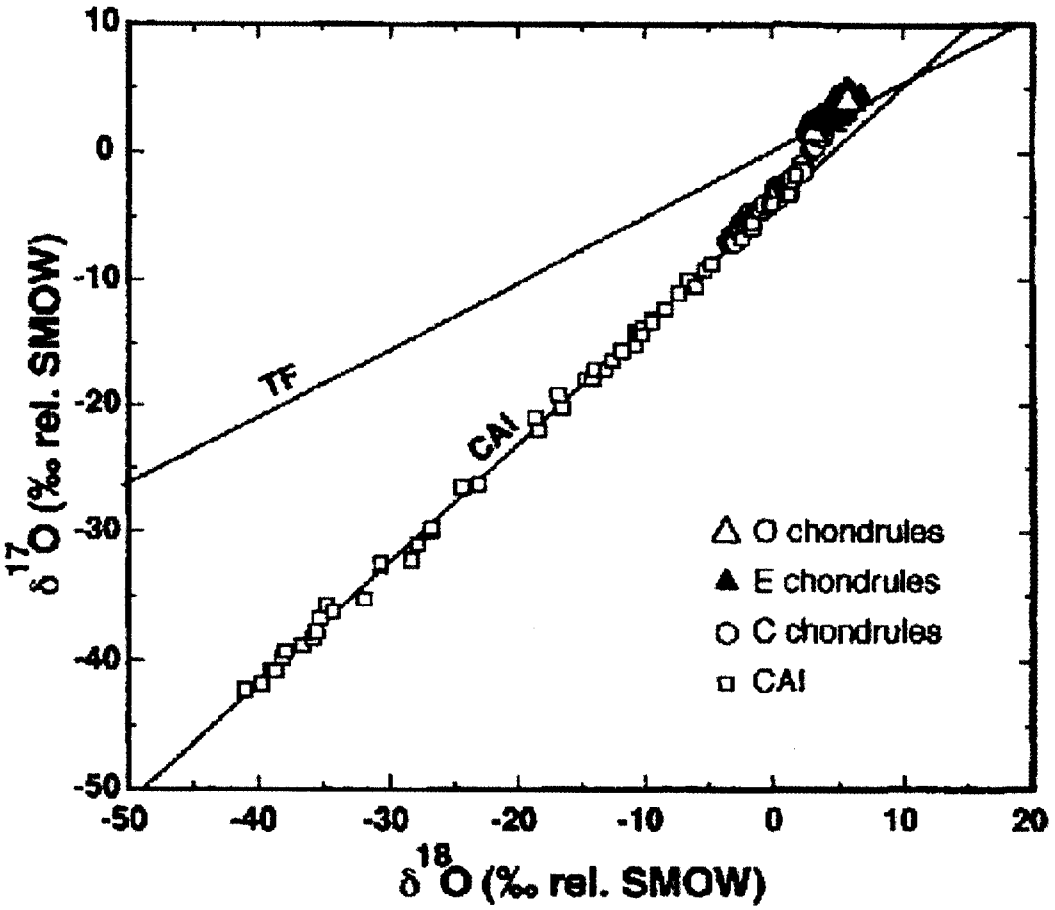

Figure 1 Mass independent fractionation of oxygen isotopes in meteorites (Clayton, 1993).

1.2. Models for the Origin of Oxygen Isotopic heterogeneity in the Solar System

Three alternative mechanisms have been proposed to explain the observed spread in oxygen isotopic compositions of the Solar System materials that follow the mass-independent fractionation line with a slope of ~1: (1) nucleosynthetic effects (Clayton et al., 1973), (2) chemical mass-independent fractionation effects (Thiemens & Heidenreich, 1983), and (3) photochemical self-shielding effects (Clayton, 2002; Yurimoto & Kuramoto, 2004; Lyons & Young, 2005).

According to the nucleosynthetic effects, the slope-1 line reflects an inherited O-isotopic heterogeneity in solar nebula materials (^{16}O-rich solids and ^{17,18}O-rich gas) resulting from either nucleosynthesis in stars (Clayton et al.,1973) or from nuclear reactions that involve energetic particles from the proto-Sun or from galactic cosmic rays (Lee, 1978). However, since isotopic variations of other elements (e.g., Mg, Si, Ca, Ti) are much smaller and uncorrelated with the O-isotopic anomaly, this mechanism appears to be unlikely (Clayton, 1993). In addition, ^{16}O-rich presolar grains are exceptionally rare in meteorites (Nagashima et al., 2004; Nittler, 2003).

According to the chemical mass-independent fractionation effects, the slope-1 line resulted from chemical mass-independent fractionation effects similar to those observed in gas-phase O_3 production (Thiemens and Heidenreich, 1983). The chemical mechanism of mass-independent fractionation in O_3 is believed to be a preferential stabilization of the asymmetric isotopologue arising from a lack of intramolecular equilibrium in the symmetric isotopologue, referred to as an η -effect (Gao et al., 2002). However, the solar nebula is too reducing for O_3 to be a significant component. Although an η -effect could also occur during SiO_2(g) formation, Marcus (2004) has argued that O + SiO $\rightarrow$ SiO_2 in the inner gas phase solar nebula will be too slow by several orders of magnitude vs. the reaction of O with H_2 to form H_2O. Instead, Marcus (2004) proposed that mass-independent fractionation occurred during SiO_2 formation on grain surface during CAI formation. This removes the spatial dependency and allows the reaction to occur anywhere in the nebula. It is known that O_3 formed on the walls of reaction vessels does not have a mass-independent fractionation signature, but how relevant that result is to SiO_2 formation, in which SiO is incorporated into the grain surface, is unclear. Experiments involving metal oxide reactions will be of importance in developing a model for the reactions in the nebula. The reactions of O + CO and OH + CO have been demonstrated to produce mass-independent isotopic effects, consistent with the proposed role in the nebula via symmetry reactions.

The third mechanism proposed for the mass-independent O-isotopic

fractionation is photochemical self-shielding effects in CO. Self-shielding in O_2 was first considered as a possible solar nebular process (Kitamura and Shimizu, 1983; Thiemens and Heidenreich, 1983). It was shown later that trapping of photodissociated O by metal atoms, H, and O_2 is inefficient compared to O-isotopic exchange reactions in the solar nebula (Navon and Wasserburg, 1985). Thiemens and Heidenreich (1983) and Navon and Wasserburg (1985) proposed that self-shielding in CO, as observed in astronomical environments, was responsible for production of the meteoritic isotopic anomalies. The isotopically selective photolysis of CO has been well known in the astronomical community for a long time (Bally and Langer, 1982; van Dishoeck and Black, 1988), and this mechanism has also been also suggested to explain the origin of the O-isotopic anomaly in meteorites and the evolution of O-isotopic compositions of the inner solar nebula (Clayton, 2002; Lyons and Young, 2005; Yurimoto and Kuramoto, 2004). Three different astrophysical settings for CO self-shielding have been proposed to account for the solar system O-isotopic anomalies: the protosolar molecular cloud (Yurimoto and Kuramoto, 2004), the inner protoplanetary disk (Clayton, 2002), and the outer protoplanetary disk (Lyons and Young, 2005).

1.3. The Purpose of this Thesis

Although it is not clear which of the models is correct, they all agree that this range of oxygen isotopic compositions is due to mixing of two isotopically distinct reservoirs – ^{16}O-rich and ^{17,18}O-rich. Although ^{16}O-rich ($\delta^{17,18}O < -70‰$) solids have been discovered in meteorites (e.g., Krot et al., 2002; Kobayashi et al., 2003), as yet there has no been evidence for the existence of ^{17,18}O-rich reservoir in the early Solar System. The purpose of this thesis is to constrain the ^{17,18}O-rich reservoir and clarify the origin of oxygen isotopic heterogeneity in the solar system.

2. EXPERIMENTAL

2.1. Isotope Microscope System

2.1.1. Overview

A novel isotope imaging technique named "isotopography" (Yurimoto et al., 2003) was used in this thesis. Therefore, the principles and features are described in this chapter.

Isotope imaging is achieved by raster-scanning and direct-imaging methods. The direct-imaging method uses stigmatic ion optics to transfer the sputtered ions from sample surface to two-dimensional ion-detector installed at the image plane of the optics with positional relationship. The spatial resolution of direct-imaging method is determined by the ion optics differ from the raster-scanning method limited by probe size. Therefore, direct-imaging method can increase probe intensity to increase the precision and shorten the measurement time without degradation of spatial resolution if the 2D detector has sufficient capability. The basic concept of direct-imaging method is illustrated with comparing to raster-scanning method in Figure 2.

Isotope microscope is an analytical instrument using a direct-imaging method that has capability of high precision isotope ratio imaging of micro-scale under high mass-resolution (Yurimoto et al., 2003). This method is achieved by the combination of a stigmatic Secondary Ion Mass Spectrometry (SIMS) instruments and a two-dimensional ion detector. Abundances of isotopes in natural materials are distributed over ranges of 6 orders of magnitude and their isotopic ratios are usually fluctuated less than percent order. In order to satisfy these conditions, a Stacked CMOS-type Active Pixel Sensor (SCAPS) has been proposed as a 2D ion detector (Yurimoto et al., 2003). High precision isotope ratio imaging of micro-scale under high mass resolution (isotopography) has been realized by the combination of a stigmatic SIMS instruments (e.g., Cameca ims-1270) and SCAPS attributed to the several features of 2D ion detection (Yurimoto et al., 2003).

The fundamental principle of SIMS is described in §2.1.2. The characteristics of SCAPS device are described comparing with conventional 2-dimentional ion detection systems in §2.1.3. The features of isotopography are summarized in §2.1.4.

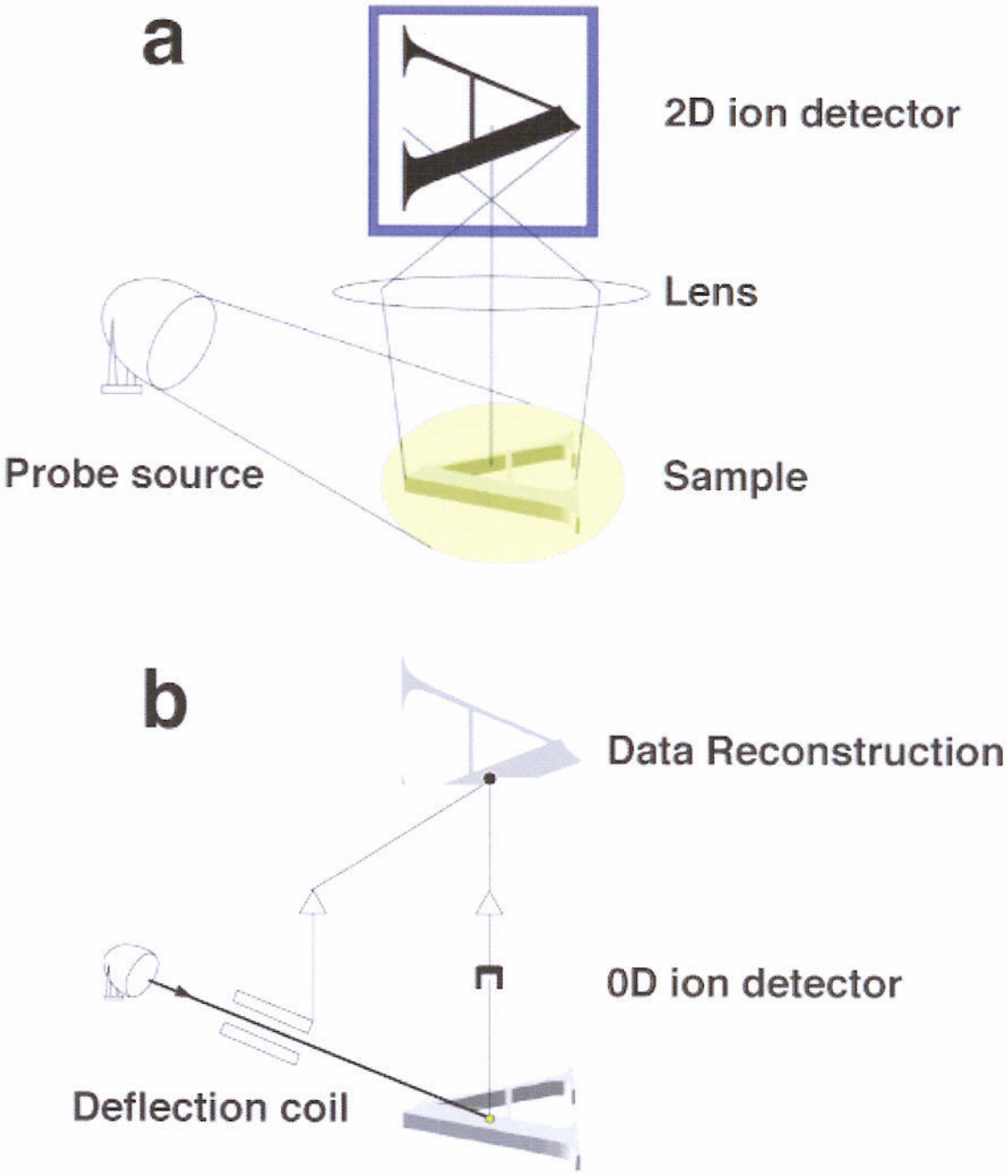

Figure 2 Illustration of isotope imaging methods. (a) Direct-imaging method (b) Scanning method

2.1.2. Secondary Ion Mass Spectrometry (SIMS)

A mass spectrometer is an instrumental to measure masses of atoms and molecules by electromagnetism. A mass spectrometer separates and determines mass-to-charge ratio (m/z) of ions after ionization of atoms. The basic parts of any mass spectrometer are composed of three parts, an ionization source, a mass analyzer and an ion detector. There are several ionization methods of atoms. In secondary ion mass spectrometry (SIMS), a focused ion beam with moderate energy (~ 1-20keV) (referred to as primary ion beam) bombarded a sample surface, and remove materials of the sample by sputtering. The sputtered materials contain ions referred as secondary ions.
A mass analyzer having magnetic sector is commonly used in SIMS. When the accelerated ions are passed through a magnetic field, Lorentz force qvB is equal to centrifugal force mv^2/r,

$$\frac{m}{q} = \frac{Br}{v} \qquad (1)$$

Where the electrostatic charge is q, velocity is v, the radius of ion's circular motion is r. When the accelerated voltage of ion is V, the ion energy is expressed $1/2mv^2 = qV$. Then equation (1) is expressed as follows:

$$\frac{m}{q} = \frac{B^2r^2}{2V} \qquad (2)$$

This equation indicates that the radius of circular motion changes with mass where the accelerate voltage V is constant. SIMS uses this effect for mass separation.
Secondary ions have variation of the energy. This variation causes chromatic aberration in the mass spectrometers. The chromatic aberration may be negated by coupling of electric field with the magnetic field. The centrifugal force $mv^2/r = 2qV/r$ of ions with energy qV is equal to electrostatic force $-q$E when E is electrostatic field strength. Then

$$\frac{2V}{r} = -E \qquad (3)$$

Ions with same energy but different to masses can be focused to one spot if we design. Such condition calls "energy focusing". On the other hand, "directional focusing" is a case that secondary ions emitted from a point with several angles are focused to another spot. "Double focusing mass spectrometer" can be performed energy focusing and directional focusing at once. The condition of double focusing can be realized when an energetic and magnetic analyzers compensate between energy dispersion caused by electric field and momentum dispersion by magnetic field.

Conventionally, SIMS is widely used to identify the isotope ratio of the average of micro-area in materials with focused point analysis. On the other hands, SIMS has a

capability of two-dimensional analysis by primary beam scanning or stigmatic optics of mass spectrometer. The features of primary beam scanning method are the high sensitivity and high dynamic range due to the use of the EM, and the ability to use high mass resolution. A spatial resolution of scanning ion image is determined by a diameter of the primary ion beam on the sample. Cameca NanoSIMS can make several tens nm order primary beam radius using Cs ion source. In order to get a small ion beam, the use of a low beam current is mandatory. Therefore scanning method takes long time to measure large area of sample. In isotope microscope, the spatial resolution is determined by the ion optics of SIMS instruments instead of the diameter of primary ion beam. The ion optics of CAMECA ims-1270 SIMS instruments has capability to obtain the ion image with the spatial resolution about 0.2 μm.

2.1.3. Stacked CMOS-type Active Pixel Sensor (SCAPS)

The projected ion image is detected by ion imaging system. The abundances of isotopic ratio in natural material are distributed over the range exceeding 10^6, and the variations are less than % order. Therefore, in order to analyze the isotopic ratio correctly, the ion detection system is needed the two-dimensional isotope ratio imaging with wide dynamic range and permil-precision.

A variety of methods have been used to record ion images. The most popular two-dimensional ion imaging system is composed of microchannel plate (MCP), fluorescent screen (FS), and charge coupled device (CCD) (Hunter *et al.*, 1991). In this system, induced charged particles are detected by the following three steps; First, charged ions are converted to electrons by the MCP. The MCP is essentially a 2-dimentional array of 10^4-10^7 miniature channels, each of which acts as an independent electron multiplier. These channels typically operate at gain of 10^3-10^5 (Wiza, 1979). Next, the electrons are converted to photons by the FS. The FS is a fiberoptic plate coated with fluorescent material such as (Zn,Cd)S called P-20. Luminescence centers in the material are excited by incident electrons and generate photons. Finally, photons are detected by CCD and output signals from CCD are proportional to the intensity of induced photons. Although this system is high sensitive detection system, it is difficult to achieve quantitative isotopic measurement because of 1) non-linearity of the FS in electrons-photons conversion. 2) narrow dynamic range of FS. 3) time dependent change of conversion efficiency of FS and MCP which is caused by damage from electron or ion bombardment. Consequently, the error in isotope analysis was limited to > 5% (Hoppe et al., 2000). In order to solve the problems of FS, resistive anode

encoder (RAE) is used in spite of the FS-CCD system (Odem *et al.,* 1983). Although this system has good response against incident ions and good sensitivity to detect single ion, multi event cannot be detected. Thus the effect of deadtime is not negligible. Therefore, it is difficult to measure high and low intensity incident ions at the same time. The system also requires MCP still exists a problem with time dependent change of conversion efficiency.

In order to overcome these difficulties, a stacked complementary metal-oxide semiconductor (CMOS)-type active pixels sensor (SCAPS) has been developed (Matsumoto et al., 1993; Yurimoto et al., 1996; Takayanagi et al., 1999; Nagashima 1997, 2000, 2001; Kunihiro et al., 2001a). Figure 3 shows the photo of SCAPS device. The SCAPS has two dimensional pixel array (600x576 pixels) and capability of direct detection of charged particles. Therefore 2D ion detection is achieved. The pixels have excellent sensitivity for several particles in particular to charged particles not only ions but also electrons (Yurimoto and Matsumoto 1996; Yurimoto et al., 1997) and soft-X-rays (Takayanagi et al., 1995). The SCAPS is integrated type detector. Therefore, there is no dead time in principle. The excellent linearity of the pixel relation of incident ions and output signals are reported (Nagashima et al., 2001) and the ultra-low noise system is constructed as a result of noise analysis of pixel structure (Kunihiro et al., 2001a). The SCAPS has high advantages over conventional systems including two-dimensional detection, wide dynamic range, no insensitive time, direct detection of charged particles, a high degree of robustness, and high fill factor (Takayanagi et al., 2003). The ion microscope using SIMS can be extended to two-dimensional isotopic ratio imaging with permil-precision by the SCAPS (Yurimoto et al., 2003).

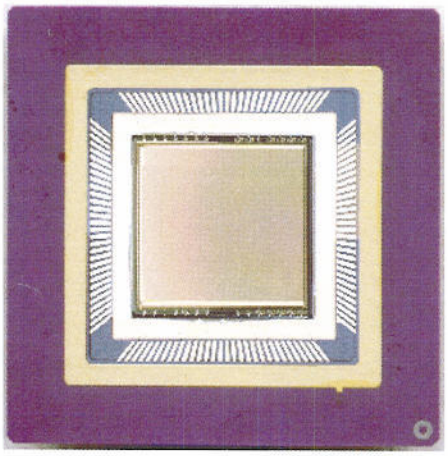

Figure 3 Chip photo of SCAPS assembled in a 121pin PGA package.

2.1.4. Isotopography

Isotopography means an analytical method of high precision isotope ratio imaging of micro-scale under high mass-resolution discuss above. Some properties of isotopography using direct combination of stigmatic-SIMS and SCPAS are listing as;

(1) High precision ion imaging can be achieved because the spatial resolution is not related to the probe intensity and the SCAPS has the wide dynamic range and excellent linearity.

(2) Direct ion detection and ultra-low noise of the system realize the quantitative analysis.

(3) Comparing conventional point analysis that require the appropriate analytical conditions such as slits or probe conditions of SIMS instruments, isotopography can fairly ignore these conditions but the adjustment of ion optics related to the blurring is needed.

(4) Isotopography can obtain only the relative value of each materials included in the isotope ratio image. In order to determine the isotope ratio value relative to the standard material, the value of any material in the image should be known. In other words, isotopography always analyze the standard material and the sample at the same time if the material that has known its isotope ratio is existed in the image.

2.2. Experimental Conditions

2.2.1. Sample Description and Preparation

A polished thin section of Acfer 094 ungrouped carbonaceous chondrite and Murchison CM2 chondrite were prepared. A carbon evaporation film of about 30 nm was coated on the thin section in order to reduce electrostatic charging during high-energy electron and ion bombardments for chemical and isotopic analyses. Figure 4 shows whole image of Acfer 094 thin section in this thesis.

Acfer 094

Acfer 094 is a unique, petrologic type 3 carbonaceous chondrite breccia with mineralogical, petrologic, nitrogen isotopic and oxygen isotopic affinities to the CM and CO groups (Newton et al., 1995; Greshake, 1997). Its bulk chemical composition is similar to that of CM chondrites, whereas oxygen isotopic composition and matrix

modal abundance are similar to those of CO chondrites. In contrast to CM chondrites, Acfer 094 shows no evidence for aqueous alteration and thermal metamorphism and has a distinctive carbon isotopic composition. Acfer 094 also has one of the highest abundances of presolar SiC, diamonds and silicate (Newton et al., 1995; Gao et al., 1996; Nagashima et al., 2004; Nguyen et al., 2004).

Murchison

Murchison is a CM2 carbonaceous chondrite. CM carbonaceous chondrites consist primarily of a mixture of anhydrous minerals (predominantly olivine and pyroxene) and phyllosilicate matrix minerals. The anhydrous phases are found both within chondrules and as isolated grains in the matrix, and are generally believed to have formed at high temperatures (as igneous minerals or as condensates), whereas the matrix phases are thought to have formed at low temperatures (< 400 K). The genetic relationship, if any, between these two groups of minerals has been a subject of study for many years.

Oxygen-isotopic data for bulk CM chondrites and mineral separates (Clayton and Mayeda, 1999) lie along a mixing line with slope ~0.7 on the three-oxygen isotope plot, implying that the water reservoir had a composition with $\Delta 17O$, the magnitude of the deviation from terrestrial fractionation line, more positive by the quantity than the silicate reservoir. Clayton and Mayeda (1999) showed that the observed patterns can be accounted for with a simple closed-system hydration reaction at temperatures near 273K, with water/rock ratios in the range 0.4-0.6 (in terms of oxygen atoms).

CM carbonaceous chondrites contain 9 wt% H_2O (Jarosewich, 1990) bound in phyllosilicates phases (mainly serpentines), clumps of serpentine-tochilinite intergrowths (previously called "poorly characterized phases" or PCP) (Tomeoka and Buseck, 1985), reflecting aqueous alteration. Most researchers have concluded that alteration took place on the CM parent asteroid (e.g., McSween, 1979a, 1987; Bunch and Chang, 1980; Barber, 1981; Tomeoka and Buseck, 1985; Zolensky and Browning, 1994; Browning et al., 2000; Trigo-Rodriguez et al., 2006) rather than in the solar nebula (e.g., Grossman and Larimer, 1974).

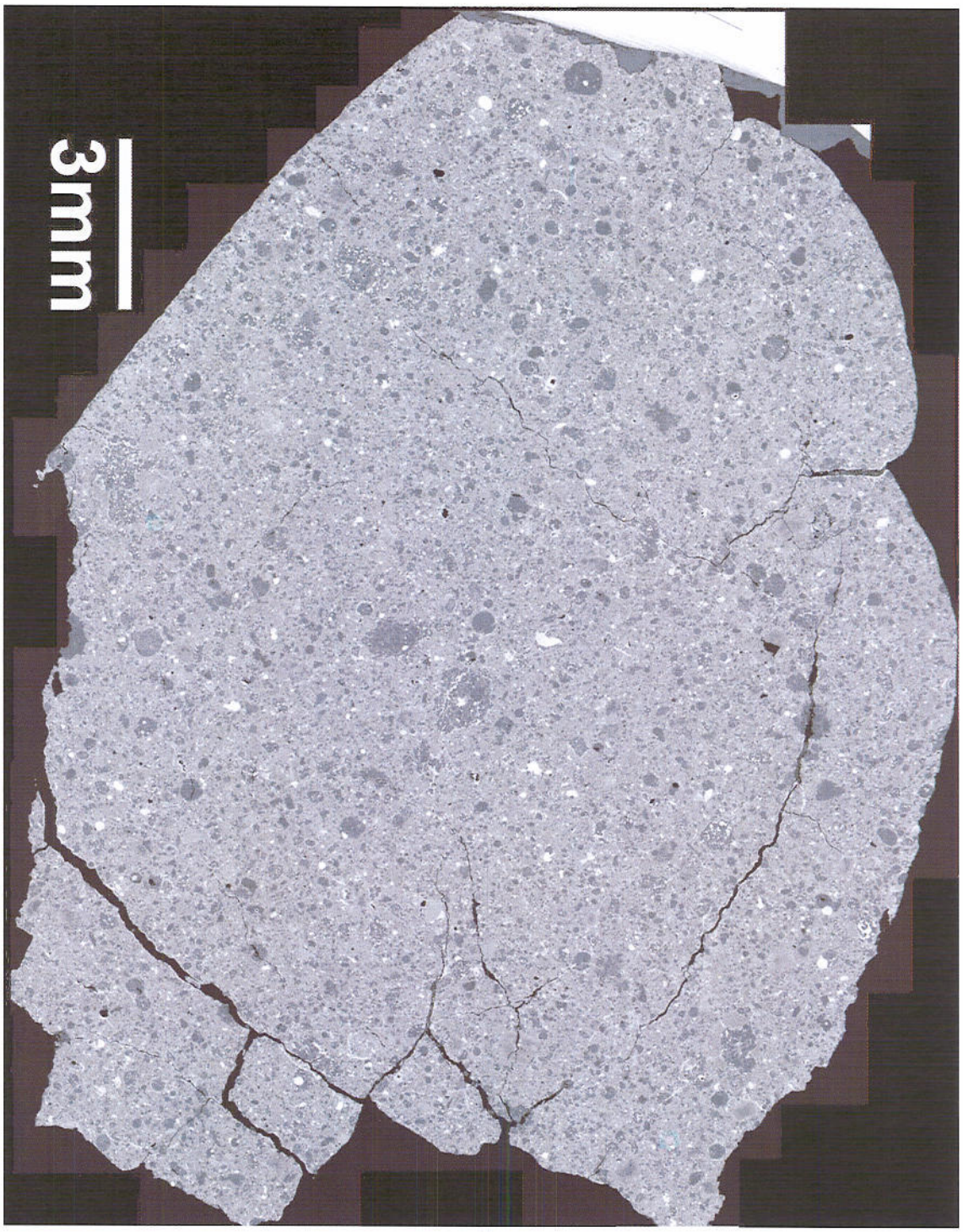

Figure 4 Backscattered electron image of Acfer 094 polished thin section.

2.2.2. Petrographic analysis

SEM-EDS

A field-emission type scanning electron microscope (FE-SEM, JEOL JSM-7000F) equipped with an energy dispersive X-ray spectrometer (EDS, Oxford INCA Energy) has been used to analyze petrographical texture and chemical compositions. The probe current was 0.9nA. A cobalt standard implanted in the sample holder was used to calibrate the signal intensity and the energy dispersion every session of analysis. And 100 μm-sized olivine and pyroxene grains in the Acfer 094 thin section were also analyzed for conformation of quantitative chemical analysis.

ATEM

An analytical transmission electron microscope (ATEM, JEOL JEM-2010) equipped with EDS (Thermo Electron Noran system SIX) has been used to analyze crystal structure, crystal size, texture and compositions. A sample for ATEM study was directly cut out from the thin section by focused ion beam (FIB) method using SII NanoTechnology SMI3050TB instrument. Figure 5 shows the sample preparation procedure for ATEM study. A TEM specimen of ~8μm x 8μm x 50 nm was also cut out from the petrographic thin section by the same FIB system, and was further gently polished on both sides by argon ion milling (accelerating voltage <1KV) to remove damaged and contaminated layers produced during the FIB cutting.

2.2.3. Isotopic analysis

Isotopography

A Hokudai isotope microscope system (Cameca ims-1270 + SCAPS; originally installed in Tokyo Institute of Technology and now in Hokkaido Univ. (Hokudai)) has been used to image precise oxygen isotope distribution (isotopography) in the meteorite matrices. A Cs^+ primary beam of 20 keV was homogeneously irradiated on the sample surface of approximately 80 μm in diameter with a beam current of ~0.3 nA. A normal incident electron gun was used to compensate positive charging of the sputtered region due to the primary beam. We obtained secondary ion images of $^{12}C^-$, $^{13}C^-$, $^{12}C^-$, $^{27}Al^-$, $^{28}Si^-$, $^{16}O^-$, $^{18}O^-$, $^{16}O^-$, $^{17}O^-$, and $^{16}O^-$ sequentially for one analytical sequence. The exposure time was 20 seconds for $^{12}C^-$, 1000 seconds for $^{13}C^-$, 100 seconds for $^{27}Al^-$, 200 seconds for $^{28}Si^-$, 20 seconds for $^{16}O^-$, 3200 seconds for $^{17}O^-$ and 1600 seconds for $^{18}O^-$ isotopography. A 50 μm contrast aperture was used and the

secondary ion contributions except for objective isotopes were cut by the exit slit. Beam irradiation time for the sequence was ~2 hour. The sputtering depth was less than 200 nm for the sequence. Typical spatial resolution under the condition of isotopography was ~0.3 μm. The width of a pixel of SCAPS corresponds to 0.2 μm on the sample surface. An image processing method of moving average with 3 × 3 pixels was applied to isotope ratio images to reduce the statistical error due to small ion integration of ^{17}O and ^{18}O. As a result, a spatial resolution of isotope ratio image is 0.6 μm, and the oxygen isotopic precision per the spatial resolution is ±25‰ (σ) for $\delta^{17}O_{SMOW}$ and ±10‰ (σ) for $\delta^{18}O_{SMOW}$. On the other hand, the standard deviations were calculated from original image without the image processing.

Point SIMS

A point analysis of SIMS has been applied to determine oxygen isotopic compositions using the Cameca ims-1270. An oval-shaped Cs^+ ion micro-probe (2.0 × 1.3 μm^2) with 20 keV was used. Secondary ions of $^{16}O^-$-tail, $^{16}O^-$, $^{17}O^-$, $^{16}OH^-$, and $^{18}O^-$ were measured by an electron multiplier (EM). The deadtime of EM is 16ns. Terrestrial magnetite and olivine standards were used to normalize secondary ion-ratios to the $d^{17,18}O_{SMOW}$-values for new-PCP and silicates, respectively.

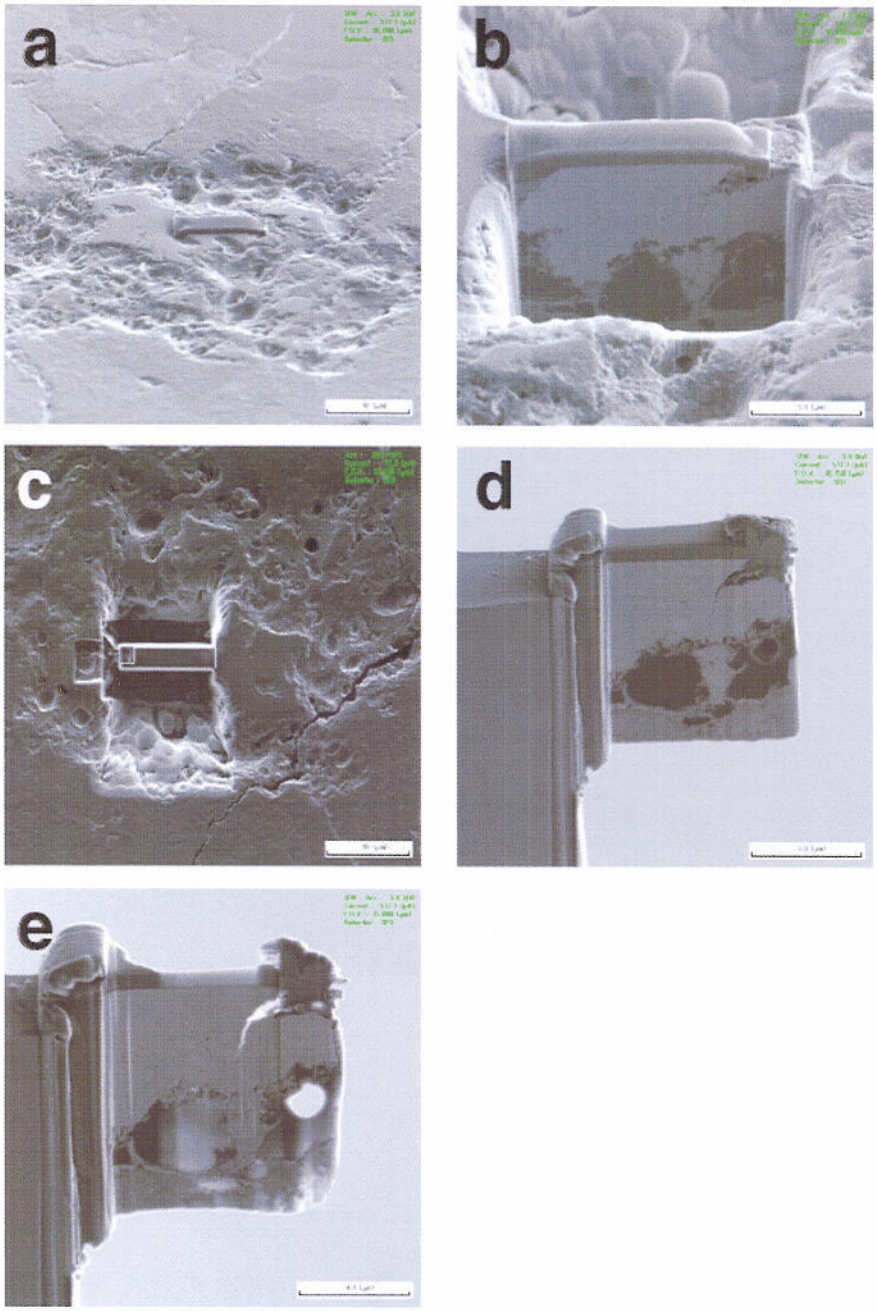

Figure 5 Sample preparation procedure with forcused ion beam instrument for the transmission electron microscopy. (a) Target region of grain #17 (see Figure 8) is protected by carbon deposit. (b) (c)Digging surrounded area by Ga ion beam. (d) Lifted up by manupirator from thin section and set to the silicon pillar (right) with carbon deposit. (e) Treated by Ar gas to reduce the damage layer after thinning by Ga ion beam. Finally the sample size become ~8 μm x 8 μm x 50nm. FIB sample preparation is assisted by T. Kaito and I. Nakatani.

3. RESULTS

3.1. Acfer 094

3.1.1. Isotopography

During our on-going in situ survey (Yurimoto *et al.*, 2003; Itoh and Yurimoto, 2003; Kunihiro *et al.*, 2005) of presolar grains of primitive meteorites (Nagashima *et al.*, 2004), we discovered isotopically anomalous regions of oxygen in matrix of the ungrouped carbonaceous chondrite Acfer 094 in addition to isotopically anomalous spots corresponding to presolar grains (Figure 6). These images were obtained at November 2004. At that time, I could not sense the ^{17,18}O-rich region because my interest was finding presolar grains, typically 0.3-μm sized particles with high anomalous oxygen isotopic compositions. Dr. Nagashima, core member of SCAPS development team, pointed out the existence of ^{17,18}O-rich region in early spring of 2005. However, the Acfer 094 sample was already returned. In March 2006, we obtained other slice of Acfer 094 and start to re-discover such ^{17,18}O-rich material. Hereafter we refer to this material as a new-PCP.

Ten new-PCP grains from Acfer 094 were analyzed by isotopography. All of new-PCP were almost equally enriched in O-17 and O-18 relative to the surrounded matrix materials (Figure 7). Previously, Kunihiro et al described quantification of isotopography. They report that the quality of isotope ratio image was estimated to equal the statistical error using pixel binning technique of 5x5 pixels corresponding to 1.25 x 1.25 μm^2 to increase the secondary ion counts in order to reduce the error. In order to quantify the true value of new-PCP, the effects of surrounded phases should be ignored. The procedure of image processing in this thesis is as follows; (1) create mask by the intensity of ^{16}O, (2) set several ROIs (typically 5 areas) (Figure 8) and average the ROI's pixels. Figure 9 shows 2-D histogram of all pixels in the δ^{18}O image including #24 grain after 5 times 3x3 moving average. The data clusters of matrix and new-PCP are produced and others are distributed between them. Figure 9 are also plotted the masked data between contours. The secondary ion intensity of new-PCP is lower than matrix. According to increase the intensity, the $\delta^{17,18}$O value decrease. The quantified values are listed in Table 1 and plotted in Figure 11 with the estimated value from isotopography.

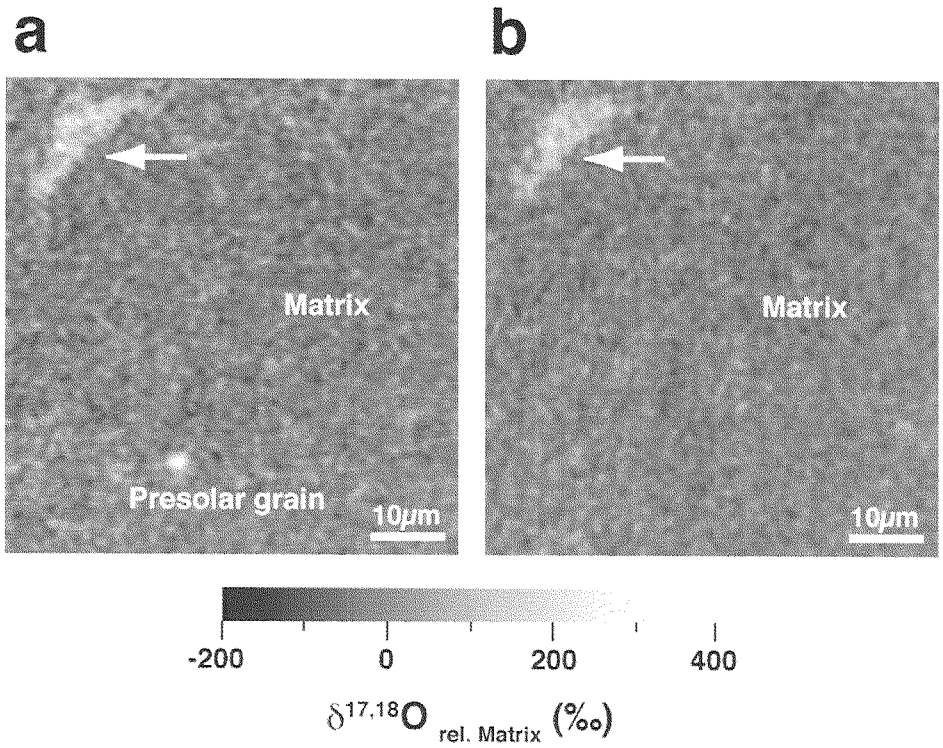

Figure 6. Spatial distribution of $^{17}O/^{16}O$ (a) and $^{18}O/^{16}O$ (b) in matrix of the ungrouped carbonaceous chondrite Acfer 094 measured using isotopography. An isotopically anomalous 10 μm-sized region and a spot are surrounded by the matrix materials. The spot corresponds to a presolar silicate grain. Arrows indicate the existence of $^{17,18}O$-rich material.

Table 1. Oxygen isotopic compositions of new-PCPs, tochilinite, matrix and AOA of meteorites. Averaging areas: # of analysis areas used for averaging. $\Delta^{17}O_{SMOW}$ $=\delta^{17}O_{SMOW} - 0.52\delta^{18}O_{SMOW}$. Isotopography: extracted from an isotope image by SCAPS using imaging SIMS. Point SIMS: measured by an electron multiplier using an oval-shaped ion micro-probe. AOA: ameoboid olivine aggregate.

Object #	Analysis area (μm²)	Averaging areas	$\delta^{17}O_{SMOW}$ (‰)	σ_{mean}	$\delta^{18}O_{SMOW}$ (‰)	σ_{mean}	$\Delta^{17}O$ (‰)
Isotopography							
new-PCP of Acfer 094							
#14	0.8 x 0.8	5	167	12	161	4	83
#15	0.8 x 0.8	5	162	13	159	2	80
#17	2.0 x 2.0	5	176	4	178	3	83
#19	0.6 x 0.4	5	148	10	152	1	69
#20	0.6 x 0.6	5	153	18	159	6	70
#21	0.4 x 0.6	3	171	9	179	4	78
#22	1.0 x 1.0	5	166	5	174	5	75
#24	1.0 x 1.0	5	182	13	192	6	82
#25	1.6 x 1.6	5	176	7	180	5	83
#27	2.0 x 2.0	5	177	2	174	5	86
Tochilinite of Murchison							
#38	2.0 x 2.0	5	-5	2	-2	3	-4
AOA of Acfer 094							
#18	3.2 x 3.2	5	-45	4	-37	2	-26
#23	4.0 x 4.0	5	-38	2	-38	1	-18
Point SIMS							
new-PCP of Acfer 094							
#17-s29	2.0 x 1.3	1	183	3	191	2	84
#17-s47	2.0 x 1.3	1	173	4	176	3	82
Matrix of Acfer 094							
#s39	2.0 x 1.3	1	2	2	1	2	1
#s40	2.0 x 1.3	1	3	2	10	2	-2
#s41	2.0 x 1.3	1	18	3	18	2	8
#s43	2.0 x 1.3	1	9	2	15	1	1
#s44	2.0 x 1.3	1	13	3	21	2	2
#s45	2.0 x 1.3	1	-7	3	0	2	-6
#s46	2.0 x 1.3	1	11	2	16	2	3
#s49	2.0 x 1.3	1	6	2	16	2	-2
mean		8	7	3	12	3	1
AOA of Acfer 094							
#s50	2.0 x 1.3	1	-44	3	-43	2	-21

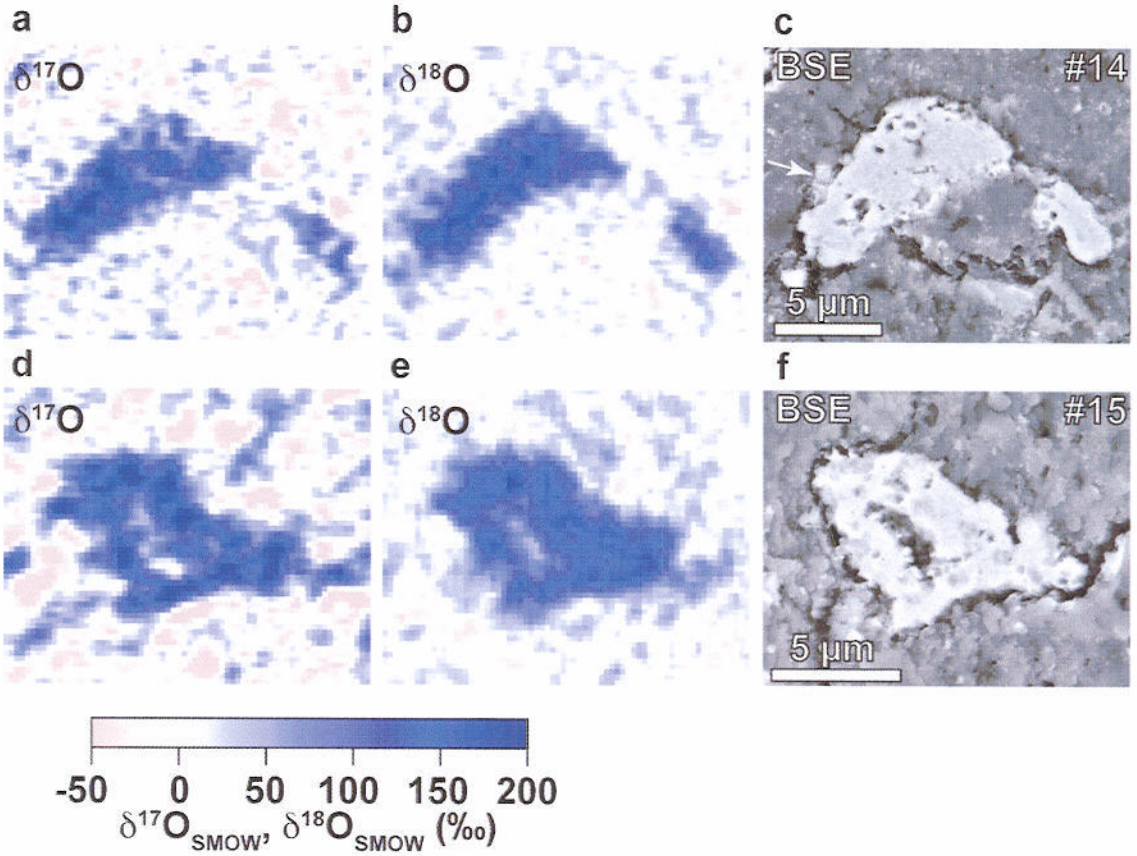

Figure 7. Oxygen isotopic distribution and grain shape for new-PCP embedded in chondrite matrix. $\delta^{17}O_{SMOW}$ (a, d, g, j, m, p, s, v, y, B), $\delta^{18}O_{SMOW}$ (b. e. h, k, n, q, t, w, z, C) and backscattered electron (c, f, i, l, o, r, u, x, A, D) images 10 for new-PCP #14 (a-c), #15 (d-f), #17 (g-i), #19 (j-l), #20 (m-o), #21 (p-r), #22 (s-u), #24 (v-x), #25 (y-A), and #27 (B-D) in the Acfer 094 matrix. Arrow in (A) indicates small troilite grains attached to the new-PCP #14. The new-PCP #21 is surrounded by troilite. Because troilite contains no oxygen, the troilite area and gaps filled with epoxy in (#17, #21, #22, #24, #25) is masked by black color. The color bar is same in all isotope ratio images. The new-PCPs are highly enriched in ^{17}O and ^{18}O isotopes relative to the matrix.

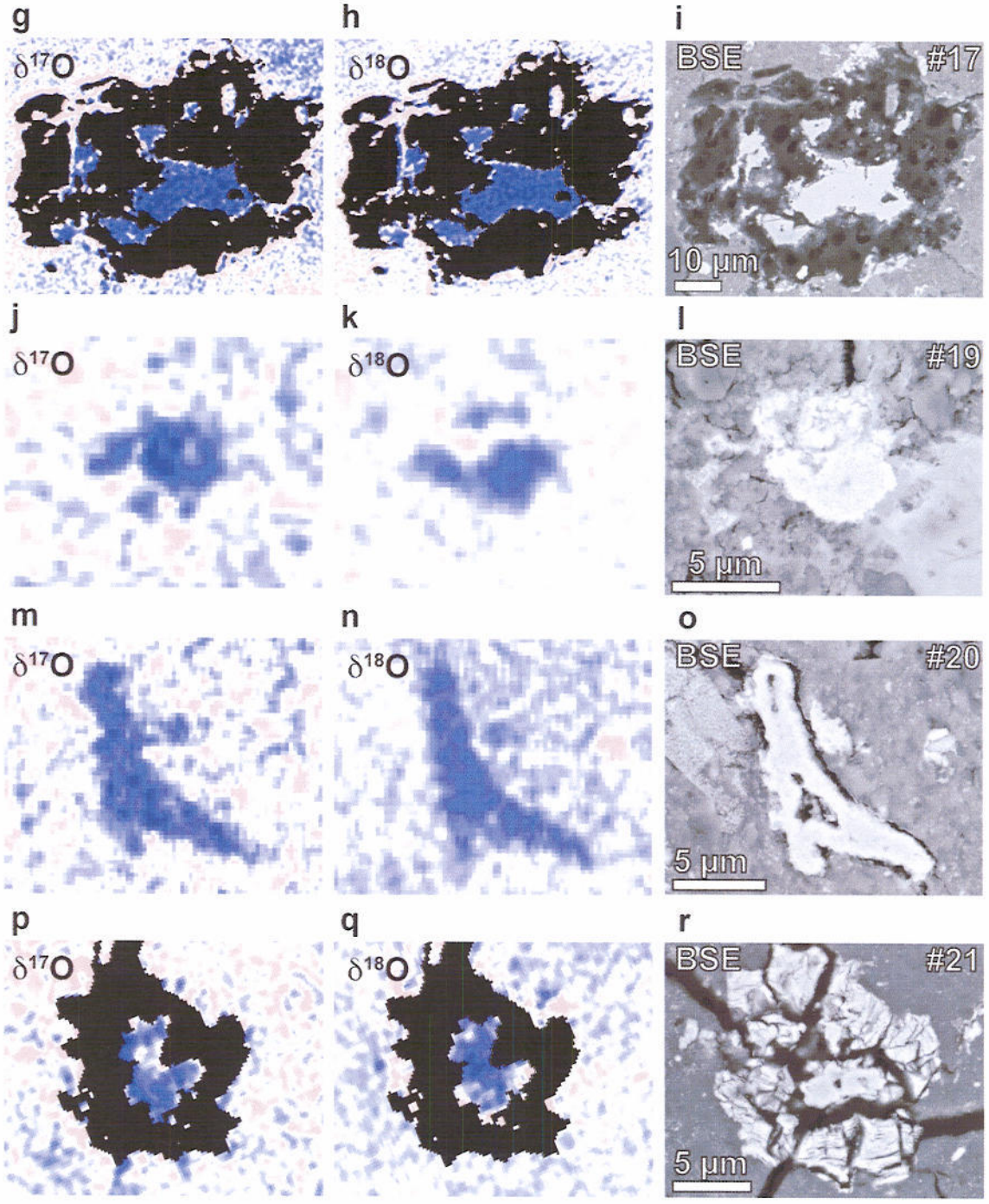

Figure 7. (continued)

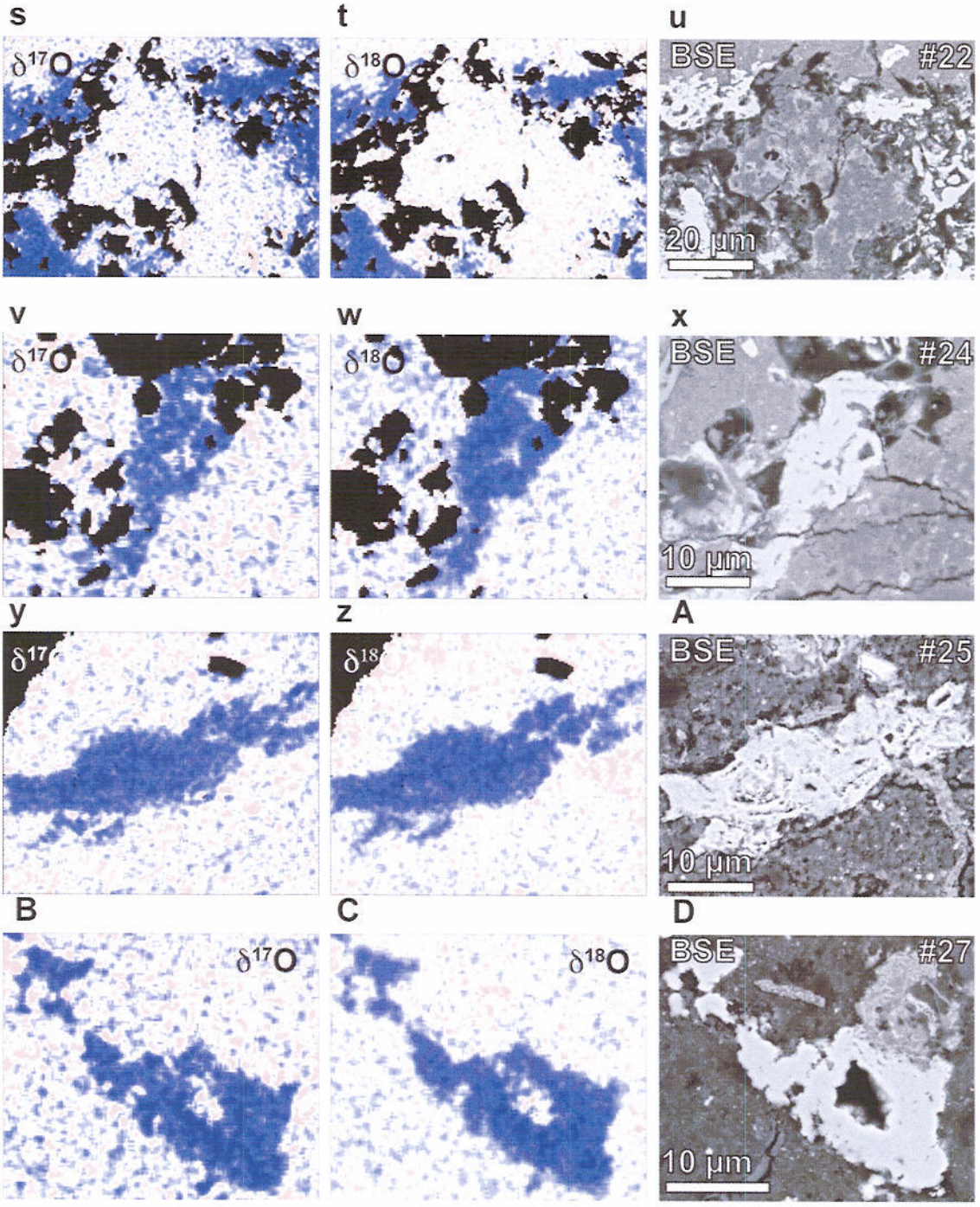

Figure 7. (continued)

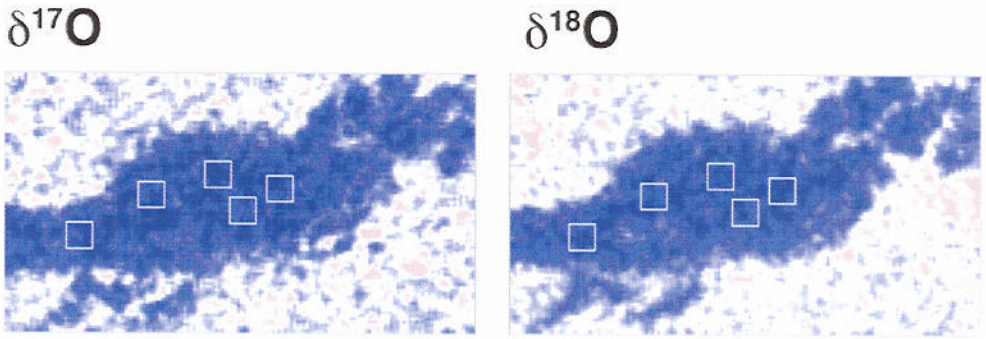

Figure 8. Example of quantification from isotope ratio images (y and z in Figure 7). White squares are selected regions of interests (ROI). The pixels of ROIs without moving averaged data are averaged to estimate the quantitative value. Color scale is same as Figure 7.

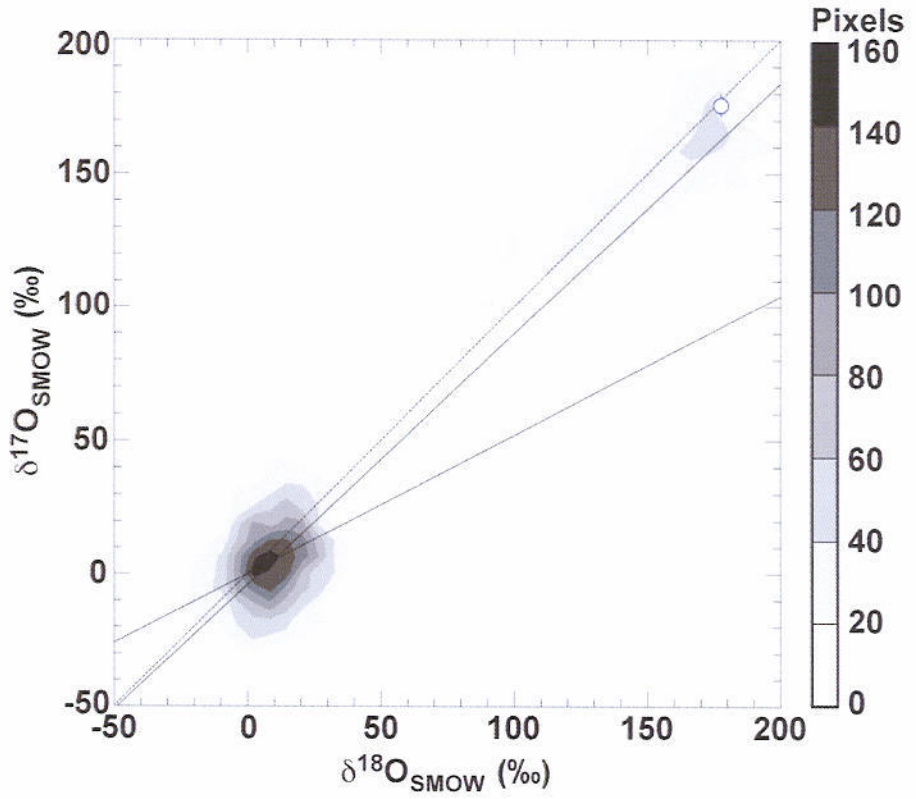

Figure 9. Comparison with two-dimensional histogram of all pixels data in the isotope ratio image from Figure 8 (contour) and average value of selected region of interests (open circle). The colors of contour mean numbers of pixels included in the range of oxygen isotopic compositions from moving averaged data.

3.1.2. Point SIMS

The new-PCP #17 grain (Figure 7i) was analyzed by point SIMS technique. In order to quantify the results of isotopography, matrix is analyzed. An amoeboid olivine aggregates (AOA) was also analyzed for references. The analyzed spots of #17 grain are shown in Figure 10. The results of point SIMS are also listed in Table 1 and plotted in Figure 11 with the estimated value from isotopography. The oxygen isotopic compositions of AOAs are enriched in 16O ($\delta^{17,18}O$=-40‰) that consistent to previous numerous works of refractory inclusions. The oxygen isotopic compositions of Matrix are plotted near the Earth along to the CCAM or slope-1 line. On the other hand, new-PCP is significantly enriched in O-17 and O-18 ($\delta^{17,18}O$=+180‰) to the CCAM or slope-1 line that consistent to the results of isotopography.

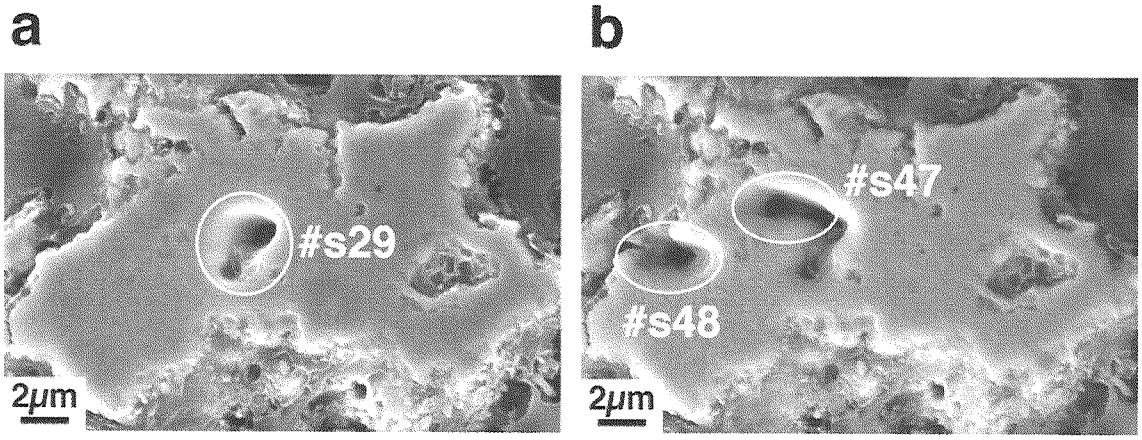

Figure 10. Secondary electron images of new-PCP #17 (Figure 7i) after point SIMS analysis. #s29 in a white circle of (a) and #s47, #s48 in (b) indicates analyzed points and probe shapes. The data of #s48 is not presented in this thesis because the isotope ratio data was unstable during measurement probably caused by the effect of surrounded epoxy.

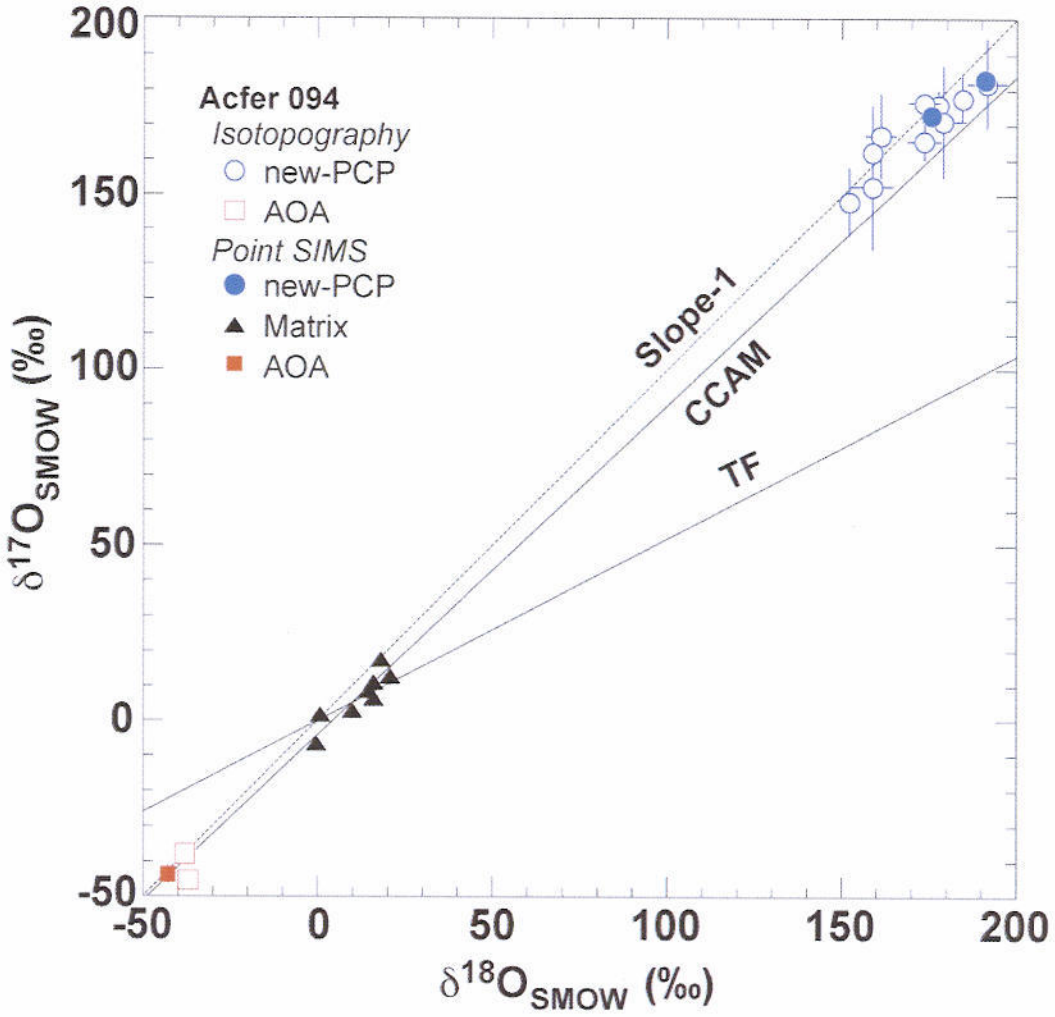

Figure 11 Oxygen isotopic compositions of the new-PCP from the Acfer 094 matrix analyzed by isotopography (open symbol) and conventional point analysis by SIMS (Point SIMS) (filled symbol). Oxygen isotopic compositions of matrix and amoeboid olivine aggregate (AOA) from Acfer 094 are also plotted. The new-PCPs are plotted on extrapolation of slope-1 line or carbonaceous chondrite anhydrous mineral mixing (CCAM) line.

3.1.3. Petrology

new-PCP

The shape of new-PCP looks bounded lashing or globule shape in few micrometer width of each lashing and some grains seem to be come loose (Figure 7). The surface of new-PCP after spattered by Cs ions shows 100nm sized intricate nanostructure (Figure 12). Because this structure corresponds to the size of fuzzy nanocrystals observed by TEM study, boundary of these nanocrystals are considered to appeared on SEM images by ion etching.

The chemical compositions of new-PCP are listed in Table 2. The chemical compositions of the isotopically anomalous regions determined by an energy dispersive X-ray spectrometer (EDS) attached to a field-emission type scanning electron microscope (FE-SEM) show that they are homogeneous and mainly composed of Fe, Ni, O and S (representatively, in wt%, Fe, 61.6; Ni, 5.4; O, 19.3; S, 9.6; Mg, 0.1; Si, 0.2). The metal-sulfide phases are estimated pyrrhotite or pentlandite according to the Ni contents.

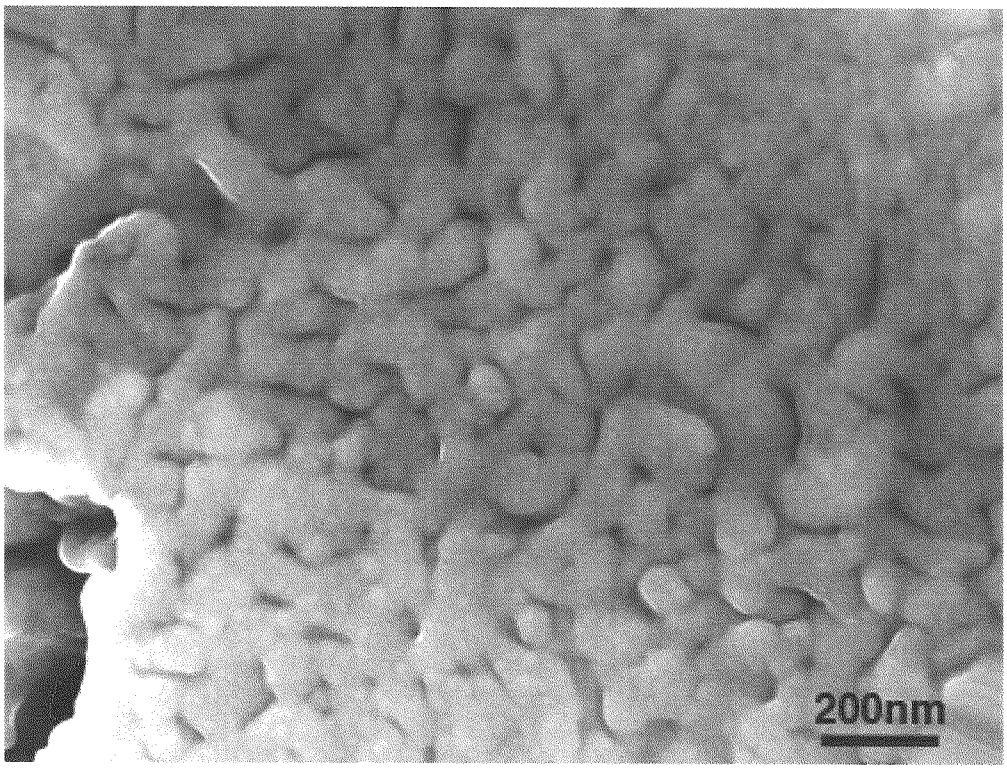

Figure 12. Secondary electron image of new-PCP #14 after spattered by Cs^+ ions.

Table 2 Chemical compositions of new-PCP and PCP. FESON: tochilinite from Tomeoka and Buseck (1985), FeO*,Fe2O3* : assumed as molar FeO:Fe2O3 =1:1 for Acfer 094 and as FeO for Murchison, Fe# : assumed as $(Fe,Ni)_9S_8$ for #17, #19, #20 , #22, #24, #25, #27, $(Fe,Ni)_7S_8$ for #14, #15, #21, and (Fe,Ni)0.9S for Murchison. n.d.: not detected. Other elements detectable by X-ray EDS are estimaed to be <0.1 weight %. S:sum of cations of oxydized atoms.

	Acfer094										Murchison	
	#14	#15	#17	#19	#20	#21	#22	#24	#25	#27	#38	FESON
Weight %												
SiO_2	0.3	1.1	n.d.	0.5	n.d.	0.3	n.d.	n.d.	n.d.	n.d.	0.3	0.8
Al_2O_3	n.d.	n.d.	n.d.	n.d.	0.2	n.d.	n.d.	n.d.	n.d.	n.d.	1.2	3.8
FeO*	22.6	22.7	22.0	21.4	21.2	22.6	21.0	20.7	21.2	21.6	33.3	24.8
Fe_2O_3*	50.2	50.5	48.9	47.6	47.2	50.2	46.6	46.0	47.2	48.1	n.d.	n.d.
MgO	n.d.	0.4	n.d.	0.0	0.2	0.2	n.d.	n.d.	n.d.	0.2	3.8	4.4
CaO	0.2	n.d.	0.1	0.2	n.d.	n.d.	n.d.	n.d.	n.d.	n.d.	n.d.	n.d.
$Fe^{\#}$	14.1	12.8	12.1	16.1	14.5	14.8	16.1	15.2	14.2	15.3	31.5	29.4
Ni	1.0	0.5	7.3	2.7	5.5	0.7	3.6	4.7	5.2	3.5	0.6	3.8
Cu	n.d.	1.3	n.d.	n.d.	n.d.	n.d.	n.d.	n.d.	n.d.	n.d.	n.d.	n.d.
S	9.9	9.5	9.7	9.5	10.0	10.2	9.9	10.1	9.7	9.5	20.5	20.8
Total	98.2	98.7	100.2	98.1	98.8	99.0	97.1	96.7	97.5	98.3	91.1	87.8
Oxidized atom #												
Si	0.12	0.48	n.d.	0.24	n.d.	0.12	n.d.	n.d.	n.d.	n.d.	0.05	0.16
Al	n.d.	n.d.	n.d.	n.d.	0.10	n.d.	n.d.	n.d.	n.d.	n.d.	0.29	0.92
Fe	24.47	25.68	24.24	24.07	22.62	23.76	22.58	21.97	23.36	24.39	5.81	4.34
Mg	n.d.	0.26	n.d.	n.d.	0.14	0.15	n.d.	n.d.	n.d.	0.13	1.18	1.35
Ca	0.10	n.d.	0.07	0.09	n.d.	n.d.	n.d.	n.d.	n.d.	n.d.	n.d.	n.d.
O	32.97	35.45	32.39	32.66	30.45	32.08	30.11	29.30	31.14	32.65	7.53	7.40
Sulfurized atom #												
Fe	6.57	6.20	5.70	7.76	6.62	6.69	7.43	6.95	6.68	7.38	7.06	6.41
Ni	0.43	0.23	3.30	1.24	2.38	0.31	1.57	2.05	2.32	1.62	0.14	0.79
Cu	n.d.	0.57	n.d.	n.d.	n.d.	n.d.	n.d.	n.d.	n.d.	n.d.	n.d.	n.d.
S ≡	8.00	8.00	8.00	8.00	8.00	8.00	8.00	8.00	8.00	8.00	8.00	8.00
Σ	24.69	26.41	24.31	24.40	22.86	24.04	22.58	21.97	23.36	24.52	7.33	6.77

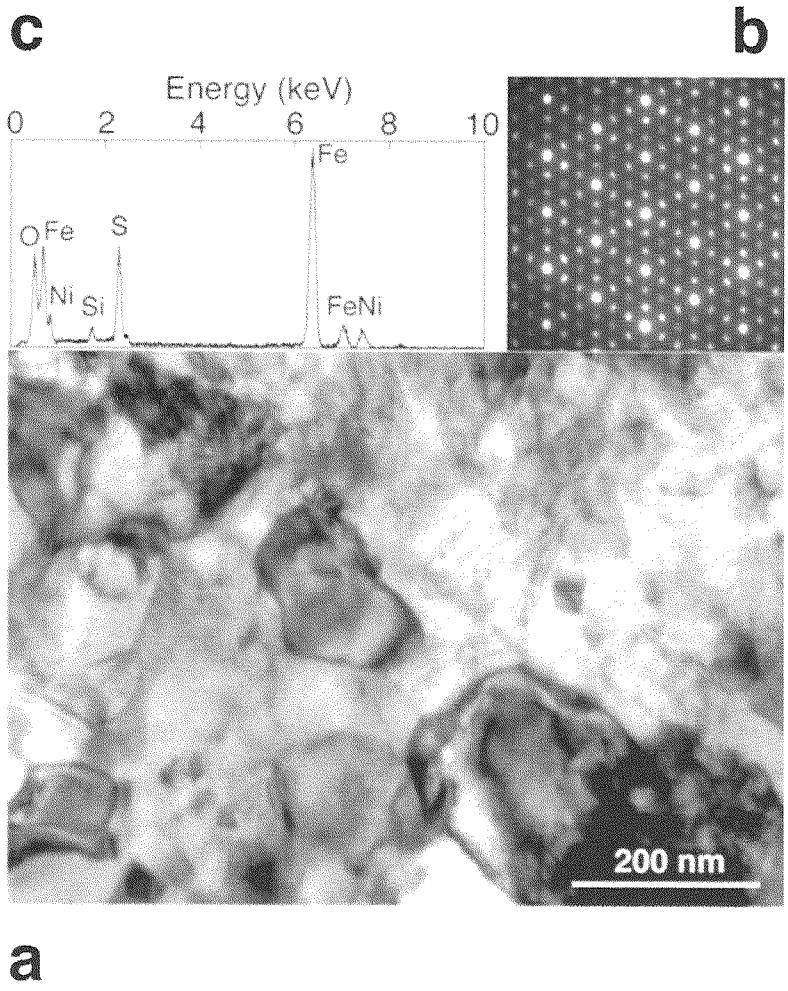

Figure 13 (a) Transmission electron micrograph showing the texture of new-PCP. (b) A diffraction pattern and (c) an X-ray elemental spectrum from a single new-PCP grain. The main spots in the diffraction pattern are similar to those of magnetite (space group Fd3m); the weak extra spots indicate a 3-fold superstructure. This pattern is viewed along [111] of the Fd3m cell of the main spots. These data are produced by Dr. Seto.

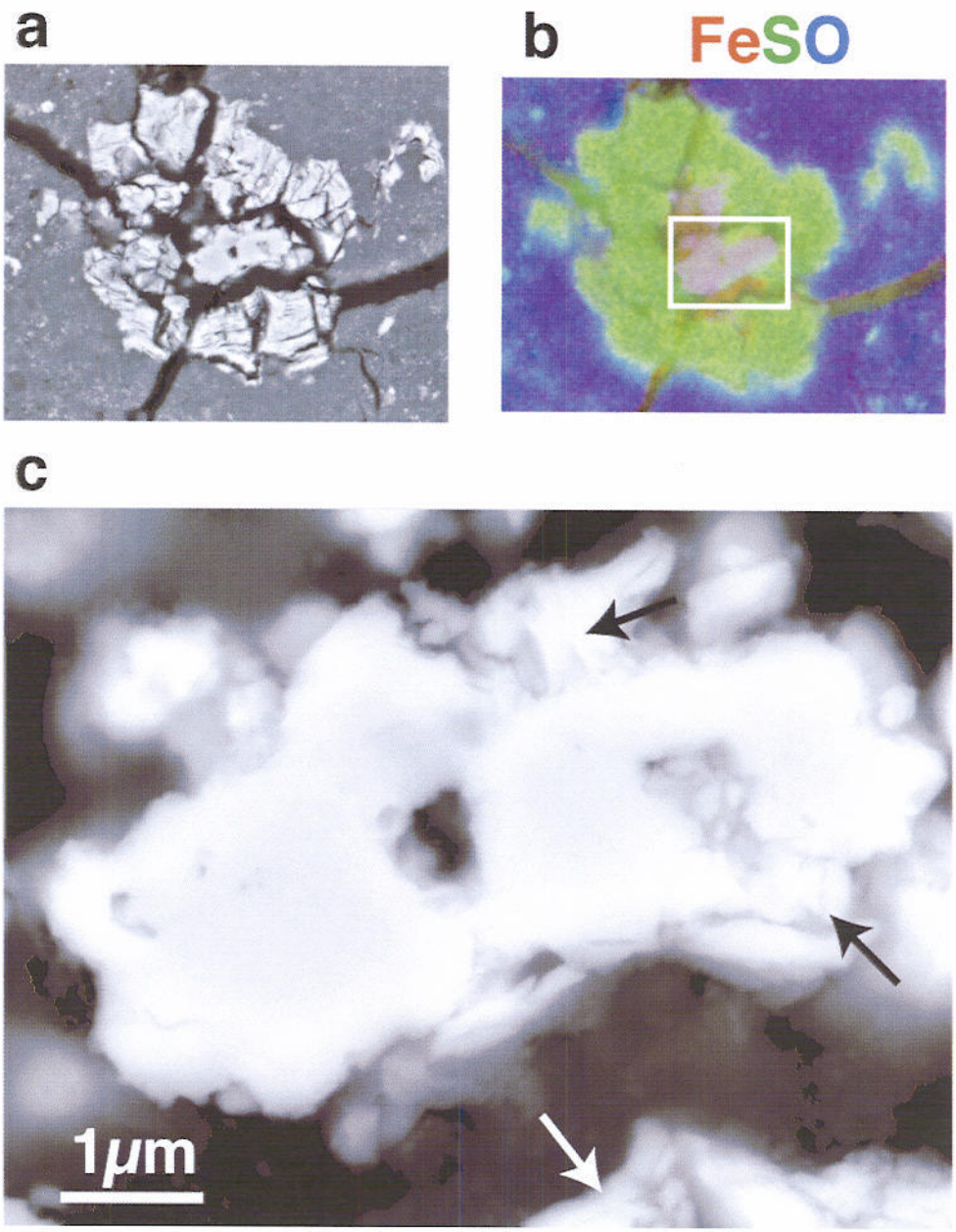

Figure 14. (a) Backscttered electron (b) X-ray Elemental map of new-PCP #21 which Fe is red, S is Green and O is blue. Purple color indicates new-PCP in (b). (c) Close up image of squared area. Arrows indicates FeS.

Iron-Nickel Monosulfides

Four types of iron-nickel sulfides were observed from Acfer 094 in this study as (1) spherical to euhedral pyrrhotite or troilite with pentlandite forming lath structure (Figure 15 a and e), (2) troilite with pentlandite filled interstices of Fe-rich olivine grains (Figure 15 b and f), (3) irregular shaped plastic troilite with granular pentilandite (Figure 15 c and g) and (4) fractured angular-shaped Fe-Ni sulfide (Figure 15 d and h). (1) was reported to generally occur as spherical to irregular-shpaed grains in the matrix and consist of troilite with pentlandite in Acfer 094 (Kimura et al., 2006). The fractured Fe-Ni sulfide grains (4) are usually, not always, attached with new-PCP and often surrounded. The bulk composition of fractured Fe,Ni-sulfides were similar to pentlandite. In contrast to ordinary pentlandite, that typically contains >20 at. % Ni, these grains attached to new-PCP have a variety of Ni contents of zero to 15 at. % whereas other types of FeNi-sulfides are clearly separated to Ni-free or Ni-rich phases. In addition, oxygen were observed about 5-20 at. % from the results of SEM-EDS study.

Iron oxides/oxyhydroxide

The fibrous habit of Fe-oxyhydroxide sometime fill the gaps between new-PCP and troilite (Figure 16). Patchy intergrowths of Fe-silicate with Fe-oxide/oxyhydroxide are also attached to new-PCP (Figure 17). The fractured troilite and a patchy texture are observed in the 100μm sized chondrule. The oxygen isotopes of the Fe-oxide/oxyhyudroxide are similar to matrix or veins. The pebbly submicron-sized sulfur-free iron grains in hydrated silicate are sometime existed near the fractured troilite attached with new-PCP. The new-PCP is partly sulfur-poor edge of lashing in submicron scale.

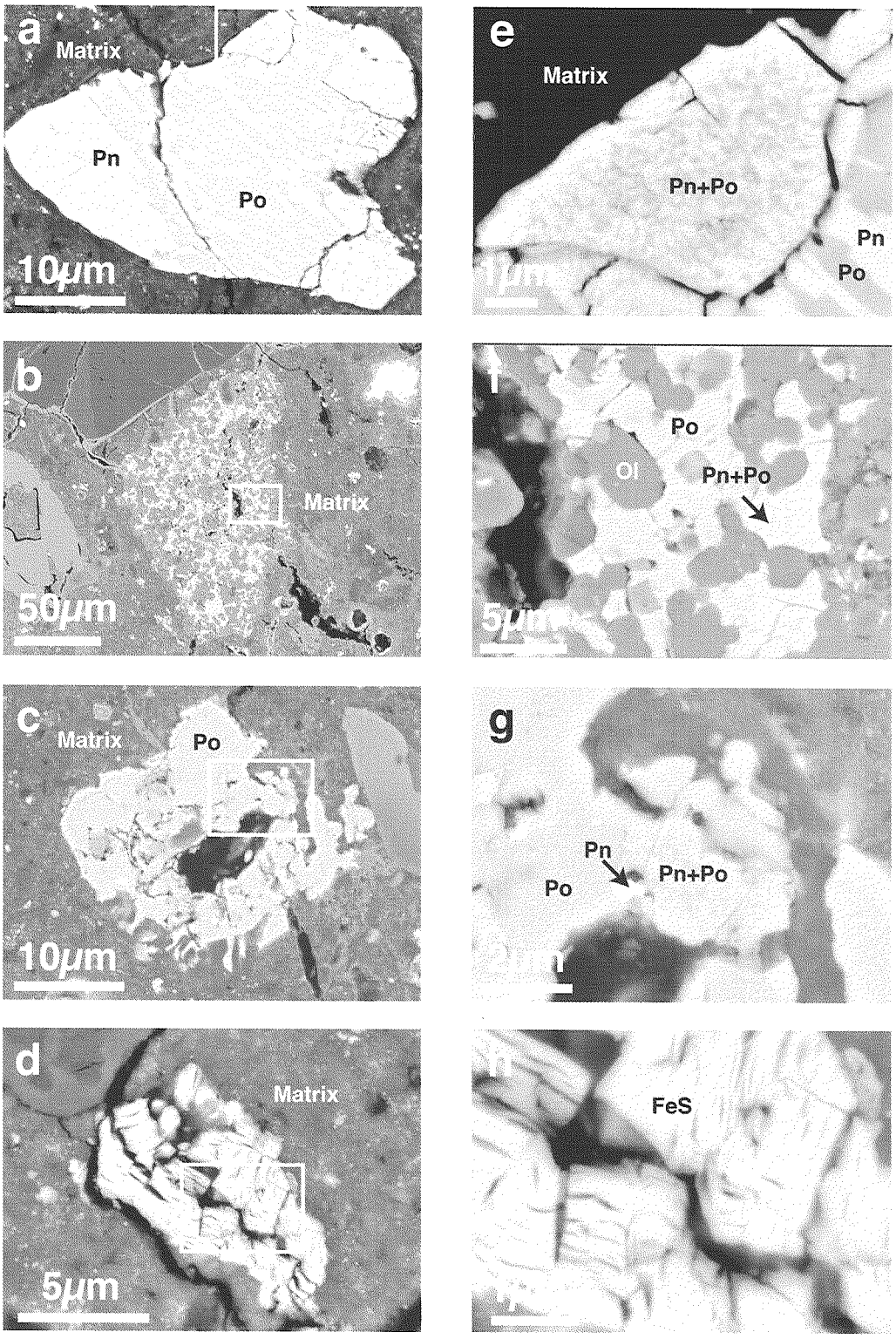

Figure 15. Different types of iron-nickel sulfides in Acfer 094 classified by the appearances. (e to h) are magnified images of square in (a to d) respectively. Pn:pentlandite, Po:pyrrhotite (or troilite), Ol:olivine, FeS: fractured FeNi-sulfide

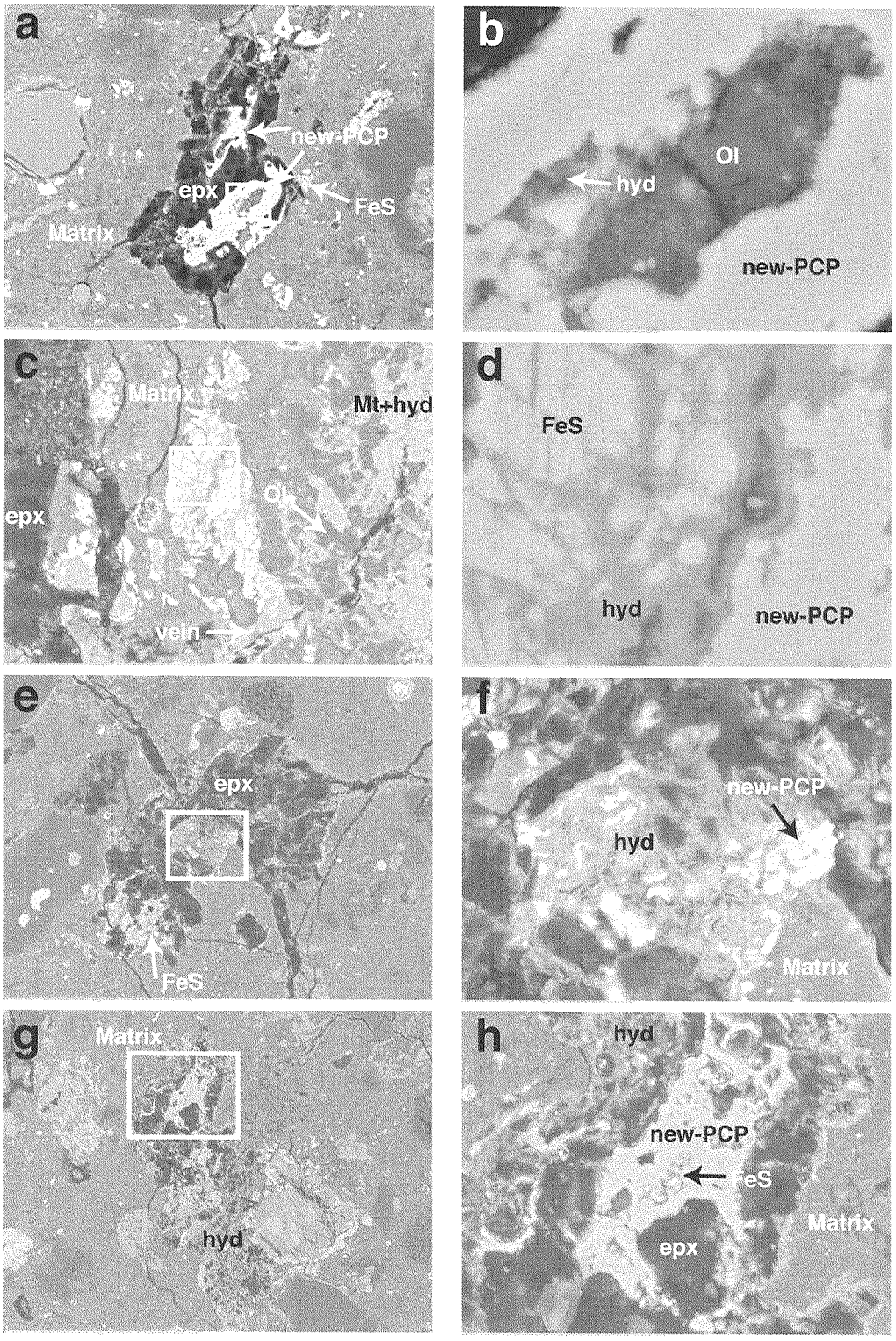

Figure 16 Morphologies of new-PCP. (b, d, f, h) are magnified images of square in (a, c, e, g) respectively. Pn:pentlandite, Po:pyrrhotite (or troilite), Ol:olivine, FeS: fractured FeNi-sulfide, hyd: Fe-oxyhydroxide, epx:epoxy

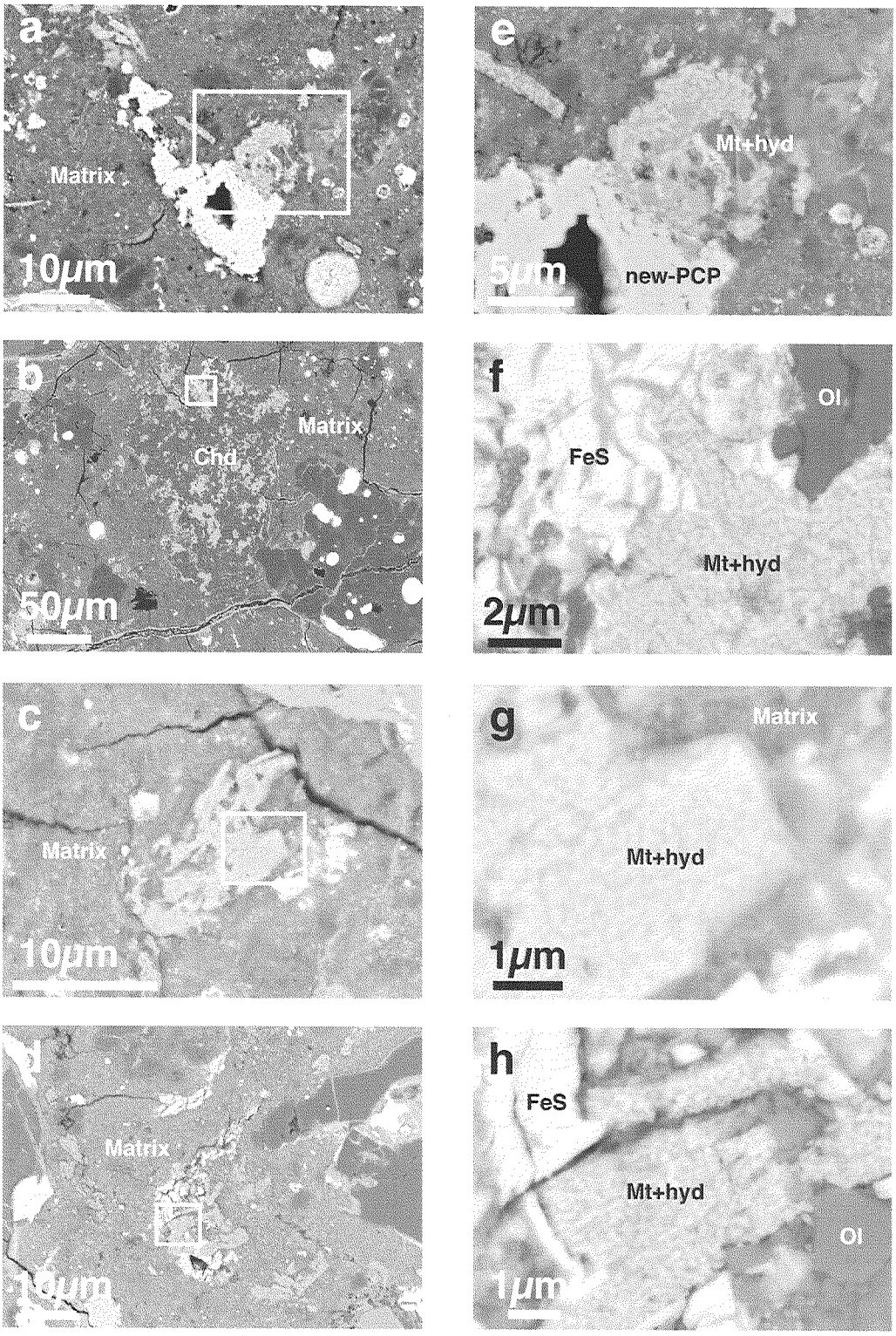

Figure 17 Granular iron oxides/hydroxides in Acfer 094. (e to h) are magnified images of square (a to d) respectively. Ol:olivine, FeS: fractured FeNi-sulfide, hyd: Fe-oxyhydroxide, Mt:sulfer-free iron oxide (magnetite)

3.1.4. Abundance

Based on the unique chemical composition of new-PCP, we have counted the new-PCP grains in an Acfer 094 thin section (Table 3). The new-PCP grains are ubiquitous and scattered randomly throughout the Acfer 094 matrix (Figure 18). In order to estimate the abundance of new-PCP, two different regions are surveyed by FE-SEM-EDS with automated grain identification program (INCA Feature). The analysis procedure is (1) automatic grain recognition under a 7-μm^2 spatial resolution with the contrast of BSE image; (2) elemental analysis of detected grains; (3) classification of the grains by the Fe, O, S contents; (4) confirmation of listed grains manually. Two analyses were performed. Twenty-two new-PCPs (the largest is 160 μm^2) were identified in 11mm^2 area of the matrix. This corresponds to 94±20 (σ) parts per million (ppm) by volume. Because the number of the new-PCP grains increases exponentially with decreasing size (Figure 19), the grain numbers below 7 μm^2 are dominant and the actual abundance of new-PCP must be larger than the estimate. The average size of identified new-PCP is 28 μm^2. Therefore, isotope imaging totally 500 μm x 500 μm area with micron resolution and an isotopic ratio precision of 1 percent would have been needed to discover a new-PCP grain when we do not know the existence of such material. This area corresponds to 100 images when a field of view of isotopography is 50 μm x 50 μm, which is the typical image size of our measurement condition.

Table 3 Abundance of new-PCP in Acfer094 matrix. The volume of Acfer 094 matrix was estimated as 62.5 vol.% of the bulk meteorites (Newton, 1995)

Run	analized area (μm^2)	count	average size (μm^2)	sigma	abundance (ppm)	grain density (count/mm^2)
A60428	3.8E+06	7	43	54	128	3.0
A60513	7.4E+06	16	22	23	77	3.4
average	5.6E+06	23	29		94	3.3

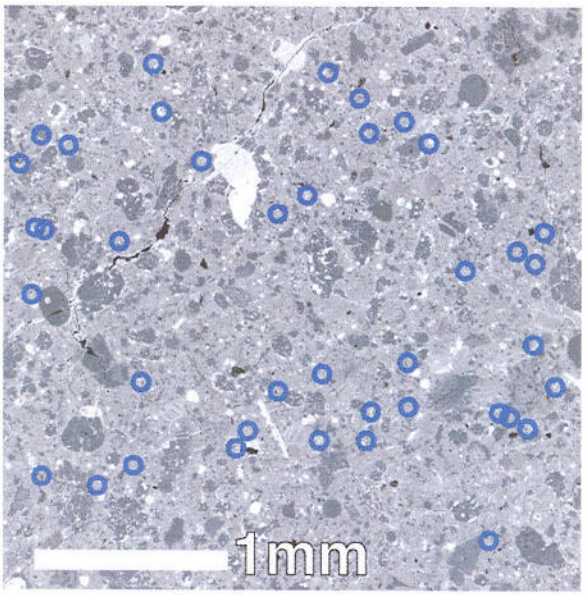

Figure 18. Spatial distributions of new-PCP in the Acfer 094 matrix. Blue circles indicate the position of new-PCP identified by the unique chemical composition.

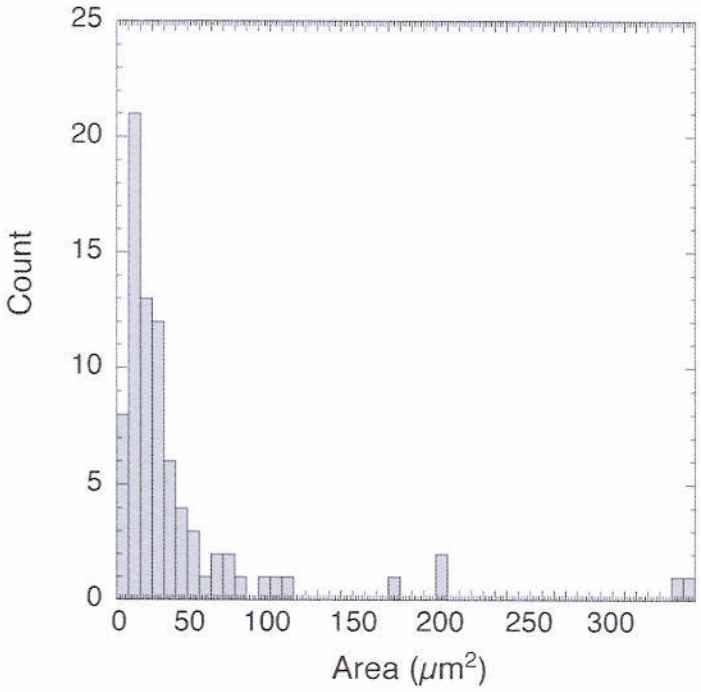

Figure 19 Size distribution of new-PCP. The bin size of this histogram is 7μm^2.

3.2. *Murchison*

3.2.1. *Isotopography*

Oxygen isotopic composition of PCP grain #38 was measured by isotopography. Figure 20 shows backscattered electron and oxygen isotope ratio images. Because spot analysis was not performed for PCP in this thesis, the oxygen isotopic composition of Murchison matrix was normalized by the literature value of Murchison matrix ($\delta^{17}O$=4.72, $\delta^{18}O$=12.70) from Clayton and Mayeda (1999). In order to quantify the oxygen isotopic composition of PCP, the magnetite standard value is also used to correct matrix effect. The result is listed in Table 1 and plotted in Figure 21. The PCP has similar oxygen isotopic composition to the matrix and along to the "CM waters" line.

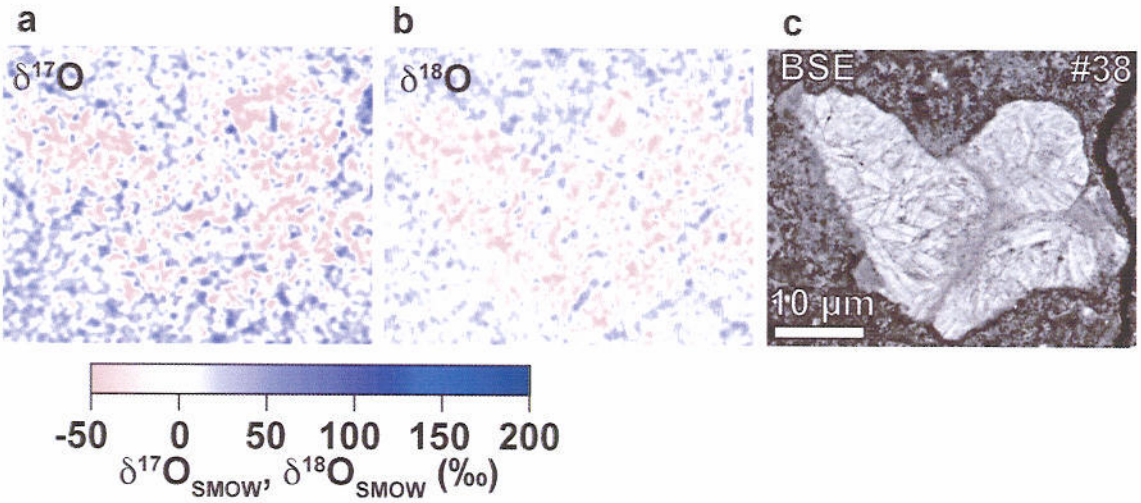

Figure 18 Oxygen isotope ratio images of $\delta^{17}O_{SMOW}$ (a), $\delta^{18}O_{SMOW}$ (b) and backscattered electron image (c) of Poorly Characterized Phase (PCP) in Murchison meteorite.

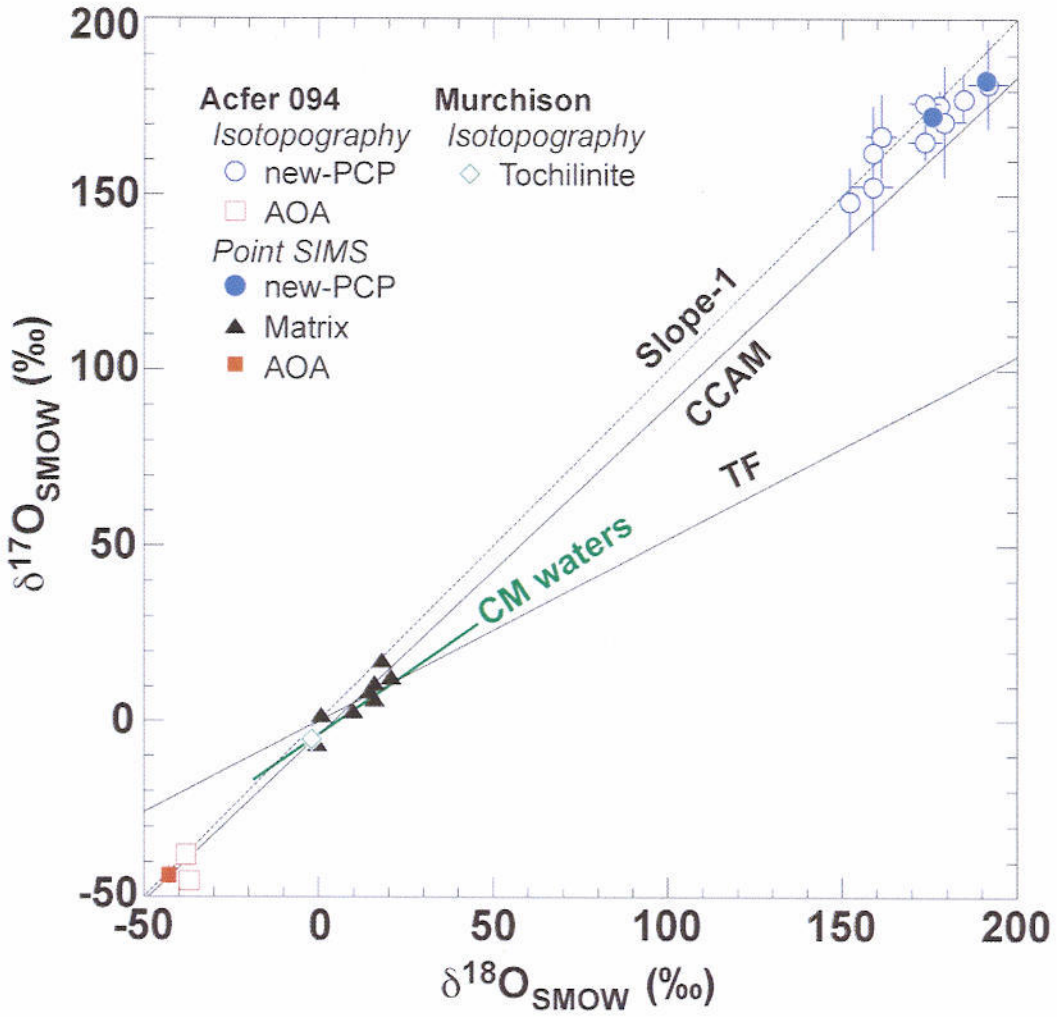

Figure 21. Oxygen isotopic compositions of tochilinite from the Murchison matrix analyzed by isotopography (green open square). The O-isotopic compositions of new-PCP and AOA, Matrix are also plotted. "CM waters" indicates the fractionation line of CM chondrites (Clayton and Mayeda, 1999). Tochilinite in Murchison meteorite is plotted around the CM waters line.

3.2.2. Petrology

Chemical compositions of PCP grain #38 from Murchison was listed in Table 2. The chemical composition is similar to Tomeoka and Buseck (1985). Although this mineral consists of the same elements as a new-PCP, its O/S atom ratios are about 4 times larger than in tochilinite. Figure 22 shows surface of PCP after isotopography. The nano scale structure observed on the surface of new-PCP is not observed in Murchison PCP. Although tochilinite shows cylindrical structure in TEM image (Tomeoka and Busek, 1985), SEM image after ion etching did not show intricate nanostructures like new-PCP.

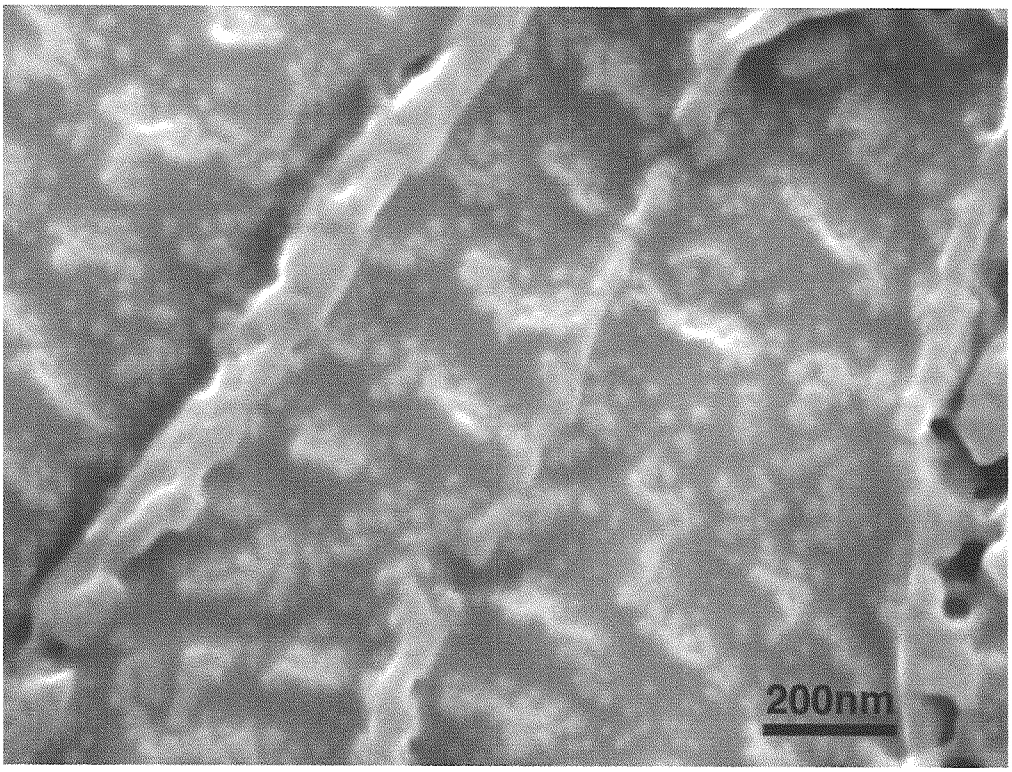

Figure 22. Secondary electron image of PCP grain #38 after spattered by Cs^+ ions

3.3. Thermodynamic calculation of Fe-O-S system

The new-PCP contained iron, sulfur and oxygen. ATEM study shows the magnetite-like structure and mixture of nanocrystals in the new-PCP. The new-PCP

often coexists with troilite (FeS). These observations suggest that magnetite and troilite are coexisted in nano-scale. The forming condition of such Fe-O-S bearing material is not reported. Therefore, we performed thermodynamic calculation of Fe-O-S system.

The new-PCP often coexists with troilite (FeS) that is considered to be a reaction product between Fe, Ni-metal and H_2S gas (Fegley, 2000; Lauretta et al., 1996).

$$Fe(s) + H_2S(g) = FeS(s) + H_2(g) \quad (4)$$

Because new-PCP has the magnetite-like diffraction patterns, magnetite can be used as its proxy. Magnetite can be formed by oxidation of Fe, Ni-metal (Fegley, 2000; Hong and Fegley, 1977) or troilite.

$$3Fe(s) + 4H_2O(g) = Fe_3O_4(s) + 4H_2(g) \quad (5)$$
$$3FeS(s) + 4H_2O(g) = Fe_3O_4(s) + 3H_2S(g) + H_2(g) \quad (6)$$

The chemical potential is defined as

$$\mu_i = \left(\partial G / \partial n_i\right)_{T,P,n} = \mu_i^0 + RT\ln a_i \quad (7)$$

where μ_i is chemical potential of phase i, G is Gibbs energy, n is number of moles of phase i and a_i is activity of phase i. The equilibrium constant expressions for these reactions are

$$K_1 = \frac{a_{FeS} f_{H_2}}{a_{Fe} f_{H_2S}} = \frac{a_{FeS} P_{H_2}}{a_{Fe} P_{H_2S}} \quad (8)$$

$$K_2 = \frac{a_{Fe_3O_4} f_{H_2}^4}{a_{Fe}^3 f_{H_2O}^4} = \frac{a_{Fe_3O_4} P_{H_2}^4}{a_{Fe}^3 P_{H_2O}^4} \quad (9)$$

$$K_3 = \frac{a_{Fe_3O_4} f_{H_2S}^3 f_{H_2}}{a_{FeS}^3 f_{H_2O}^4} = \frac{a_{Fe_3O_4} P_{H_2S}^3 P_{H_2}}{a_{FeS}^3 P_{H_2O}^4} \quad (10)$$

where f_i is the fugacity of gas i, and P_i is the partial pressure of gas i. Hydrogen and H_2O behave as ideal gases under nebular conditions, so their fugacity can be replaced by their partial pressures. Because there is no change in the number of gas molecules in all reactions, this system is independent on total pressure of the solar nebula. Reaction (5) is independent on partial pressure ratio of H_2 and H_2S gases as P_{H2}/P_{H2S}. Reaction

(6) is controlled by a partial presser ratio of $P_{H2O}^4/(P_{H2S}^3/P_{H2})$. The equilibrium constant expression of reaction (6) can be rewritten by (9) and (10) as a function of P_{H2S}/P_{H2}. The equilibriums constant Ki is calculated from the JANAF thermodynamic data. This ratio can be rewritten as $(5\times10^{-4})/(P_{H2}/P_{H2S})^3$ because P_{H2O}/P_{H2} ratio in solar nebula gas is nearly constant ($\sim5\times10^{-4}$) (Krot *et al.*, 2000). Therefore, Reactions (4), (5) and (6) are shown in a diagram of P_{H2S}/P_{H2} vs. temperature (Figure 23). According to this diagram, oxidation and sulfurization of troilite or metal would occur below 360K in the typical solar nebula. If the nebular P_{H2O}/P_{H2} ratio increases from a characteristic value for a gas of solar composition, this reaction occurs at higher temperature.

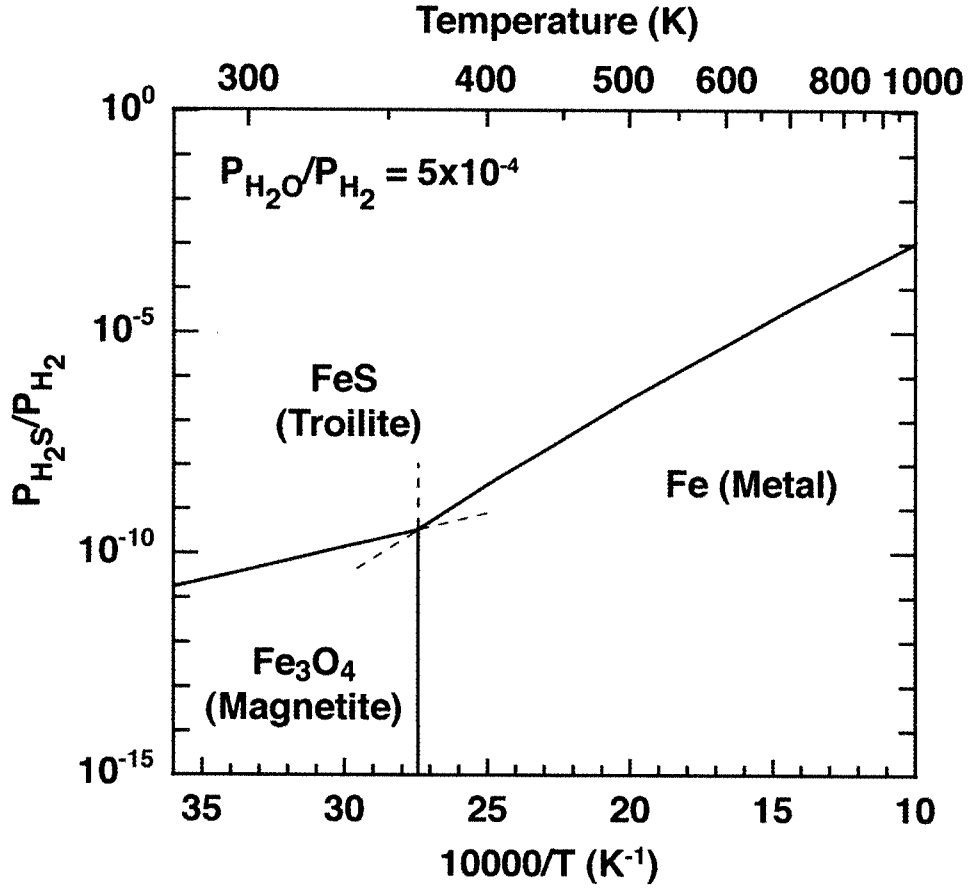

Figure 23. Calculated equilibrium temperatures for Fe-metal, troilite (FeS) and magnetite (Fe_3O_4) as a function of P_{H2S}/P_{H2} ratio. The magnetite phase boundary is calculated assuming canonical solar nebular H_2O/H_2 ratio of $5x10^{-4}$ (Krot et al., 2000). Magnetite is considered as a proxy of a new-PCP. Thermodynamic data from JANAF tables (Chase, 1998) were used for calculations.

4. DISCUSSION

4.1. Characteristics of new-PCP

Oxygen isotopic composition

The results of isotopic and petrolographic study for ^{17,18}O-rich material are summarized as; (1) highly enriched in ^{17}O and ^{18}O up to $\delta^{17,18}O$= +180‰, (2) mainly composed of iron, oxygen, (3) consist of aggregates of nanocrystals with a size range of 10-200 nm which have magnetite-like structure with 3-fold superstructure indicated by ATEM, (4) often coexisting with fractured troilite (FeS), (5) scattered randomly and ubiquitously in the Acfer 094 matrix with the abundance of 94 ppm by volume under 7-μm^2 spatial resolution survey.

Previously reported materials enriched in ^{17,18}O were magnetite (which formed by aqueous alteration of metal in the parent asteroid) in Semarkona unequiblated ordinaly chondrite ($\delta^{17,18}O$= +10‰) (Choi et al., 1998) and surface layers of metal grain in lunar soil ($\delta^{17,18}O$= +50‰) (Ireland et al., 2006). Although the oxygen isotopic composition of magnetite in Ningqiang carbonaceous chondite was reported to be enriched in ^{17,18}O (but not enriched than the Earth) than silicates (Choi and Wasson, 2003), the anomaly of lunar metal grains was not found subsequent analysis (Ireland et al., 2007). In addition, Hashizume and Chaussidon reported contrary results of the lunar metal grains ($\delta^{17,18}O$= -20‰). Clayton and Mayeda inferred that the oxygen isotopic composition of water alter the phyllosilicates in CI and CM carbonaceous chondrites were enriched in ^{17,18}O up to about +30‰ by comparison with anhydrous minerals in these meteorites. The self-shielding models propose H_2O was enriched in ^{17,18}O. The estimated oxygen isotopic composition of the primordial H_2O is $\delta^{17,18}O_{SMOW}$ = + 50‰ in Lyons and Young, (2005) and $\delta^{17,18}O_{SMOW}$ = + 200‰ in Yurimoto and Kuramoto (2004). The oxygen isotopic compositions of new-PCP are richest in ^{17,18}O previously reported. The oxygen isotopic compositions of new ^{17,18}O–rich end member are consistent with the predicted value of a self-shielding model by Yurimoto and Kuramoto. The oxygen isotopic fractionation of the solar system is expanded three times larger than previously reported.

The interesting thing is that the all of discovered materials enriched in ^{17,18}O are metal-related. In contrast, ^{16}O-rich materials are frequently discovered as silicates. Metal-related materials such as magnetite would tend to hold the oxygen isotopic composition of the ^{17,18}O-rich reservoir.

Iron-Nickel Monosulfides

The morphology of fractured FeNi sulfide grains and pentlandite like composition with low Ni constens were similar to be previously reported grains in interplanetary dust particles (IDPs) (Dai and Bradley, 2001). They found the FeNi sulfides (~2 x 5μm) has "spinel-like" cubic (Fd3m) structure with bulk composition similar to that of pentlandite ([Fe,Ni]9S8). According to {200} reflection in the electron diffraction patterns and comparison with simulated patterns suggest that the fractured grains in IDPs were not cubic (Fm3m) pentlandite ($[Fe,Ni]_9S_8$). Gamma iron sulfide (Fe2S3), greigite (Fe_3S_4) and pyrrhotite were excluded by the inconsistency of the compositor. Mackinawite (FeS(1-x), 0.07>x>0.04) with space group P4/nmm was also excluded. They reported the cubic sulfide transforms into hexagonal pyrrotite when heatetd in the electron beam. The study of the hydrated IDPs suggested a diffraction pattern from a low-Ni pentlandite grain (< atom % Ni), indexed in terms of Fm3m pentlandite (Tomeoka and Buseck, 1984). A crystallographically similar Ni-free pentlandite has been synthesized in the laboratory by low temperature (<200℃), low-pressure vapor phase growth (Nakazawa *et al.*, 1973). Pentlandite with a small amount of cobalt is known to have a cubic unit cell with a space grouping of Fm3m and the lattice constant increases with increasing iron content between 9.973 Å and 10.05 Å and the lattice constant of cubic iron sulfide is 10.5 Å explained by the complete substitution of nickel by iron in pentlandite structure.

The fractured troilite and a patchy texture are observed in the 100-μm sized chondrule (Figure 17). The oxygen isotopes of the Fe-oxide/oxyhyudroxide is similar to matrix or veins. This texture may be caused by terrestrial/planetesimal weathering. The pebbly submicron-sized sulfur-free iron grains in hydrated silicate are sometime existed near the fractured troilite attached with new-PCP. The new-PCP is partly sulfur-poor edge of lashing in submicron scale. Desulphurization would occur on the boundary between new-PCP and altered matrix followed by the aggregate of iron-oxide grains in hydrous phases. The oxygen isotopic composition of the altered phase is same as matrix. This is probably originated by fractured troilite. Previous study of weathering in hot deserts (Acfer 094 was from hot deserts) shows similar texture of troilite in ordinary chondrites (Lee and Bland, 2003). The oxygen isotopic composition of the altered phase is same as matrix. This texture may be caused by terrestrial/planetesimal weathering. No evidence of aqueous alteration of Acfer 094 (Greshake., 1997), these altered texture as observed has probably weathering effect on the Earth.

4.2. *Formation Environments of new-PCP*

4.2.1. *Solar nebula*

In order to consider the formation process of new-PCP in the Solar Nebula, the selection of oxidant is important. The dominant oxygen fraction in the Solar Nebula is CO and H_2O and mass balance dictates that ~15% of total oxygen is bound in rock (Krot et al., 2000). The proportion of H_2O to CO depends on the partitioning of carbon between CO and CH4 via the net thermochemical reaction and on the amount of oxygen consumed by rock-forming elements.

$$CO + 3H_2 = H_2O + CH_4 \tag{11}$$

In solar nebula, dominant gas phase reaction is

$$H_2O(g) + CH_4(g) = CO(g) + 3H_2(g) \tag{12}$$

Direction of Reaction (4) is calculated by below reaction data.

$$C(s) + 2H_2(g) = CH_4(g) \quad \Delta G^0_{(1)} = -69120 + 22.25T\ln T - 65.34T(J) \tag{13}$$

$$H_2(g) + \frac{1}{2}O_2(g) = H_2O(g) \quad \Delta G^0_{(2)} = -246000 + 54.8T(J) \tag{14}$$

$$C(s) + \frac{1}{2}O_2(g) = CO(g) \quad \Delta G^0_{(2)} = -111700 - 87.65T(J) \tag{15}$$

Because reaction (4) is obtained by (7) – (5) – (6), the Gibbs energy of reaction (4) is described as

$$\Delta G^0 = \Delta G^0_{(3)} - \Delta G^0_{(1)} - \Delta G^0_{(2)} = 203420 - 22.25T\ln T - 77.11T \tag{16}$$

$$\ln K_p = -\frac{\Delta G^0}{RT} = -\frac{24466}{T} + 2.676\ln T + 9.274 \tag{17}$$

Heat of reaction ΔH^0 is calculated by Gibbs-Helmholtz equation

$$\frac{\Delta G^0}{T} = \frac{203420}{T} - 22.25\ln T - 77.11 \tag{18}$$

$$\left[\frac{\partial(\Delta G/T)}{\partial T}\right]_P = -\frac{203420}{T^2} - \frac{22.25}{T} = -\frac{\Delta H^0}{T^2} \quad \Delta H^0 = 203420 + 22.25T(J) \quad (19)$$

The kinetics of the CO -> CH4 conversion are so slow that reaction (4) is quenched at very high temperatures. As a consequence, CO remains the dominant carbon gas throughout the solar nebula, and the H2O/H2 ratio remains constant at ~5x10-4 until water ice condenses. The water ice condensation point is pressure dependent and varies from ~150K at 10-7 bar total pressure to ~190K at 10-3 bar total pressure.

However, a complete chemical equilibrium the CO/H_2O ratio decreases dramatically with decreasing temperature, because reaction (12) proceeds toward the right. Eventually, $CO/H_2O << 1$ and H_2O becomes the dominant oxidant. The oxygen released from CO increases the H_2O abundance almost twofold. However, as demonstrated by Lewis and Prinn (1980), the kinetics of the CO $\rightarrow$ CH_4 conversion area so slow that reaction (4) is quenched at very high temperature. As a consequence, CO remains the dominant oxidant throughout the solar nebula, and the H2O/H2 ratio remains constant at $\sim 5x10^{-4}$. Fischer-Tropsch catalysis is the family of surface chemical reactions in which CO and H_2 are converted to hydrocarbons using transition metal catalysts. Fischer-Tropsch-type (FTT) reactions were suggested as a possible mechanism to form meteorite organics (Studier et al., 1968; Anders et al., 1973; Hayatsu and Anders, 1981) and magnetite (Fe_3O_4) can be produced in the Solar Nebular life time if the metal grains as catalysts are small (0.1 to 1 μm). However FTT reactions were also suggested that the sulfides acted as catalysts (e.g. Llorca & Casanova, 2000), iron carbide (e.g. Fe_3C) and graphite were eventually produced and poisoned as active catalysts by carbon buildup on their surface.

If the new-PCP oxidized by CO gas from small iron or FeS particles as catalysts, appreciable quantities carbon should be contained in its nanostructure, but carbon was not observed in the new-PCP. Although the new-PCP may have undergone subsequent chemical modification to remove carbon, the mechanism to removing and filling the void is unclear. Although such reactions could potentially occur within an asteroidal parent body, maximum temperatures experienced by Acfer 094 are unlikely to have been higher than effective environment for FFT reactions. Therefore, CO gas would be inappropriate as an oxidant to form the new-PCP.

The water vapor (H_2O) is the major oxidant in the solar nebula. Petrologic study and thermodynamic calculation suggests that new-PCP is formed around the reaction line between troilite and magnetite. Oxidation of troilite or metal to form new-

PCP would occur below 360K independent on total pressure of the solar nebula. If the nebular P_{H2O}/P_{H2} ratio increases, formation of new-PCP occurs at higher temperature. Although, the complete chemical equilibrium would not be expected in the cool solar nebula (Fegley, 2000), the new-PCP would be formed inside the water sublimation front (snowline) of the solar nebula because water vapor is the major oxidant in the solar nebula and the sublimation temperature of water ice is below 200K even in the several-fold H_2O-enriched nebula (Fegley, 2000). Therefore, the oxygen isotopic composition of nebular water would be preserved in the new-PCP. The observation of water vapor in the inner region of young nebula also supports this idea (Eisner, 2007). In order to test this scenario, synthetic experiment to form new-PCP like structure should be needed under controlling the fugacity of H_2, H_2S, H_2O with iron or FeS.

4.2.2. Parent body

Alternatively, the new-PCP may have been formed by aqueous alteration of metal and troilite on the Acfer 094 parent body, like tochilinite in the aqueous altered CM chondrites[16]. The new-PCP has anomalous oxygen isotopic composition whereas the oxygen isotopic composition of tochilinite is along "the CM waters" line, which is considered to be a reaction path between aqueous solution and matrix silicates toward the isotope equilibrium (Clayton and Mayeda, 1999). Therefore, the conventional aqueous alteration models are excluded for the formation process of new-PCP. The lack of mineralogical and petrographical evidence of aqueous alteration of Acfer 094 (Greshake, 1997) also supports the non-conventional alteration model. If the new-PCP were formed in a planetesimal setting, a plausible oxidant would be water vapor or aqueous solution that originated from accreted nebular ice and did not experience oxygen isotope exchange with the matrix silicates.

4.3. Oxygen isotopic composition of primordial water in the early Solar System

Because all the oxygen of magnetite is come from H_2O, the original isotopic composition of H_2O can be estimated by the fractionation factor of magnetite-water liquid-water vapor if the new-PCP was formed by oxidization or solidification of metal or troilite with H_2O. The fractionation factor of magnetite-water liquid (Zheng and Simon, 1991) and water liquid-water vapor (Majoube, 1971) in 273.5 K to 373 K was used in this calculation (Figure 24). The enrichment factor of the water estimated is almost constant in the range of this temperature as $d^{18}O$ of about -12‰ relative to that

of the new-PCP. As a result, the oxygen isotopic composition of water vapor seems to be plotted along the slope-1 line rather than CCAM line.

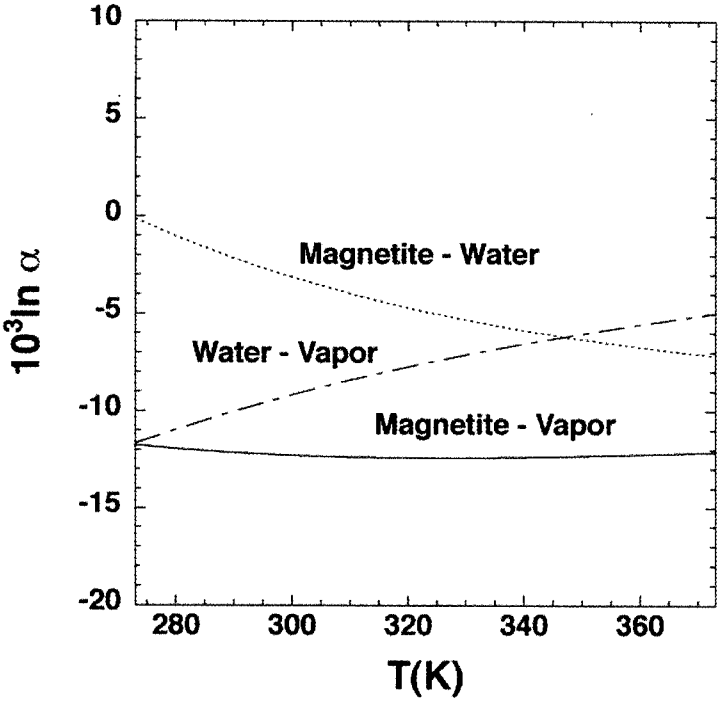

Figure 24. Isotopic fractionation factors ($^{18}O/^{16}O$) between magnetite and water liquid or vapor. α is $^{18}O/^{16}O$ ratios fractionation between phases.

In either case, solar nebula or parent body, the oxygen isotopic composition of nebula water would be preserved in the new-PCP that is the new $^{17,18}O$-rich end-member ($\delta^{17,18}O_{SMOW}$= +180‰) of the Solar System. Therefore, the oxygen isotopic compositions of new-PCP in Acfer 094 represent composition of the primordial water of the Solar System and the previously hypothesized ^{17}O- and ^{18}O-rich reservoir in the early Solar System. The wide oxygen isotopic variations of at least -80‰ $<\delta^{17,18}O <$ +180‰ found from hot and cold origin materials must provide new guidelines for the origin of oxygen isotope anomaly in the solar system. Figure 25 shows hypothesized oxygen isotopic composition by the self-shielding models and previously reported $^{17,18}O$-rich materials. The oxygen isotopic composition of new-PCP is clearly $^{17,18}O$ richest in the solar nebula. The inferred oxygen isotopic compositions (Clayton and

Mayeda, 1999; Young, 2001) and the observational most ^{17,18}O-rich composition (Choi et al., 1998) of chondrite-parent body silicates water may have recorded equilibration of aqueous solutions with the chondrite matrix and the original water before mixed with silicates in the parent body would have ^{17,18}O-rich oxygen isotopic composition like the new-PCP.

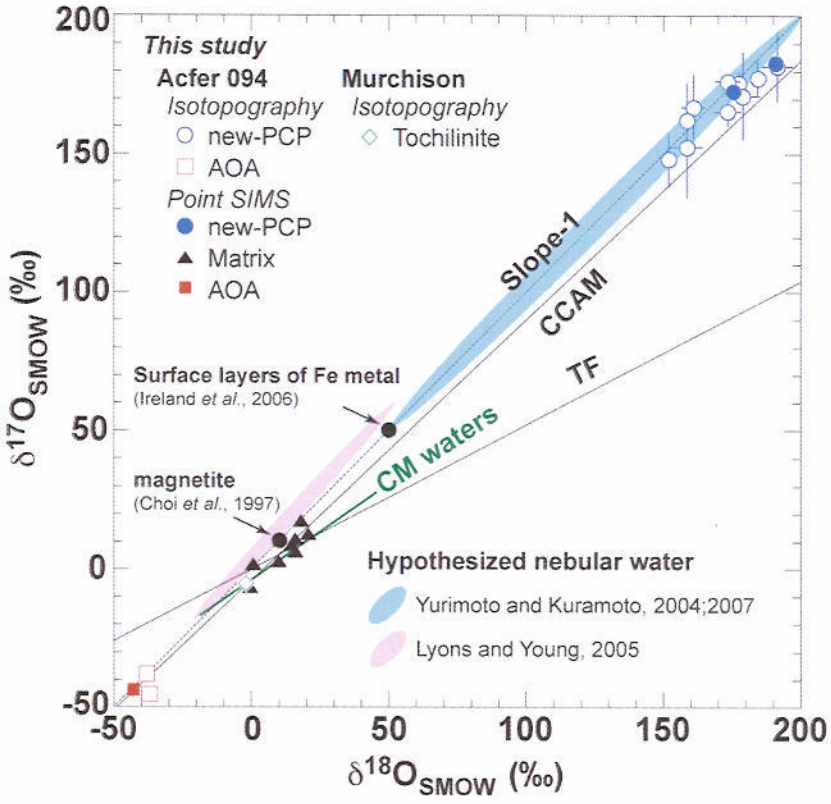

Figure 25. Oxygen isotopic compositions of the results of this study and previously reported ^{17,18}O-rich material. Hypothesized ranges of self-shielding models are also plotted.

5. CONCLUSION

New ^{17,18}O-rich reservoir ($\delta^{17,18}O_{SMOW}$=+180‰) was discovered from a unique material consisting of Fe(Ni)-O-S embedded in the ungrouped carbonaceous chondrite Acfer 094. The unique material would be resulted from oxidation of iron-metal or iron-sulfide by water. The water was extremely enriched in ^{17}O and ^{18}O corresponding to nebular water. The isotopically heavy water is consistent with the primordial water in the Solar System hypothesized by the self-shielding models, in excellent agreement with Yurimoto and Kuramoto (2004).

Acknowledgements

The author would like to express his sincere appreciation and gratitude to Dr.Yurimoto, under whose guidance the work was conducted He deeply thank to Dr.Nagashima, Dr. Kunihiro and Dr.Itoh. Much of my knowledge of SIMS, astrophysics, instrumentation and posture to research are directly introduced by them. He is also greatly indebted to Dr.Seto, Dr.Kuramoto, Dr.Fujino, Dr.Nagashima, Dr.A.N.Krot for encouragement and many useful suggestions and discussions. He also expresses his thanks to Mr. Ebata, Mr. Kobayashi for his encouragement and helpful discussions. He also thanks to members of Yurimoto-laboratory for encouragement and discussions

REFERENCES

Anders E., Hayatsu R., Studier M. H. Organic Compounds in Meteorites. *Science, 182,* 781-790 (1973).

Bally J. and Langer W. D. Isotope-selective photodestruction of carbon monoxide. *Astrophys. J., 255,* 143_148 (1982).

Barber D. J. Matrix phyllosilicates and associated minerals in C2M carbonaceous chondrites. Geochim. Cosmochim. Acta 45, 945–970 (1981).

Browning L., McSween H. Y., and Zolensky M. E. On the origin of rim textures surrounding anhydrous silicate grains in CM carbonaceous chondrites. Meteorit. Planet. Sci. 35, 1015–1023 (2000).

Bunch T., and Chang S. Carbonaceous chondrites—II: carbonaceous chondrite phyllosilicates and light element geochemistry as indicators of parent body processes and surface conditions. Geochim. Cosmochim. Acta 44, 1543–1577 (1980).

Choi B.-G., McKeegan K. D., Krot A. N., and Wasson J. T. Extreme oxygen-isotope compositions in magnetite from unequilibrated ordinary chondrites. *Nature* **392,** 577-579 (1998).

Choi B.-G and Wasson J. T. Microscale oxygen isotopic exchange and magnetite formation in the Ningqiang anomalous carbonaceous chondrite. Geochim. Cosmochim. Acta 67, 4655–4660 (2003).

Clayton R. N., Grossman L., and Mayeda T. K. A Component of Primitive Nuclear Composition in Carbonaceous Meteorites. *Science, 182,* 485-488 (1973).

Clayton, R. N. (1993) Oxygen isotopes in meteorites. *Annu. Rev. Earth Planet. Sci.* 21, 115-149.

Clayton, R. N. & Mayeda, T. K. Oxygen isotope studies of carbonaceous chondrites. *Geochim. Cosmochim. Acta* 63, 2089-2104 (1999).

Clayton, R. N. Self-shielding in the solar nebula. *Nature* 415, 860-861 (2002).

Clayton, R. N. Meteorites and Their Parent Asteroids. *Science* 313, 1743 - 1744 (2006).

Eisner J. A. Water vapour and hydrogen in the terrestrial-planet-forming region of a protoplanetary disk. N*ature* 447, 562 - 564 (2007)

Fuchs, L. H., Olsen, E. & Jensen, K. J. Mineralogy, mineral-chemistry, and composition of the Murchison (C2) meteorite. *Smison. Contrib. Earth Sci.* 10, 1-39 (1973).

Fegley, B., Jr. Kinetics of gas-grain reactions in the solar nebula. *Space Sci. Rev.* 92,

177-200 (2000).

Gao X., Amari S., Messenger S.R., Nittler L.R., Swan P. and Walker R.M.. Survey of Circumstellar Grains in the Unique Carbonaceous Chondrite ACFER 094*Meteoritics and Planet. Sci.* (1996)

Gao Y. Q., Chen W.-C., and Marcus R. A. A theoretical study of ozone isotopic effects using a modified ab initio potential_energy surface. *J. Chem. Phys., 117,* 1536_1543 (2002).

Greshake, A. The primitive matrix components of the unique carbonaceous chondrite Acfer 094: a TEM study. *Geochim. Cosmochim. Acta* 61, 437-452 (1997).

Grossman L., and Larimer J. W. Early chemical history of the solar system. Rev. Geophys. Space Phys. 12, 71–104 (1974).

Hayatsu R. and Anders E. Organic compounds in meteorites and their origins. *Topics in Current Chemistry*, 99, 1-37 (1981).

Hashizume K. and Chaussidon M. A non-terrestrial 16O-rich isotopic composition for the protosolar nebula. *Nature, 434,* 619_622 (2005).

Hong, Y. & Fegley, B., Jr. . Experimental studies of magnetite formation in the solar nebula. . *Meteorit. Planet. Sci.* 33, 1101-1112 (1997).

Hunter J. L., Linton R. W. and Griffis D. P. High dynamic range quantitative image depth profiling of boron in patterned silicon dioxide on silicon. *J. Vacuum Sci. Technol. A* 9(3), 1622 (1991).

Hoppe P., Strebel R., Eberhard P., Amari S., and Lewis R. S. Isotopic properties of silicon carbide X grains from the Murchison meteorite in the size range 0.5-1.5 μm.*Meteroritics Planet. Sci.* 35, 1157-1176 (2000).

Ireland, T. R., Holden, P., Norman, M. D. & Clarke, J. Isotopic enhancements of ^{17}O and ^{18}O from solar wind particles in the lunar regolith. *Nature* 440, 776-778 (2006).

Ireland, T. R., Holden, P., Norman, M. D., Mya J. & A. splund M. Soils ain't soils: The preservation of solar wind in metal grains from the lunar regolith. *Lunar and Planetary Science XXXVIII,* abstract #1449 (2007).

Itoh, S. & Yurimoto, H. Contemporaneous formation of chondrules and refractory inclusions in the early Solar System. *Nature* 423, 728-731 (2003).

Jarosewich E. Chemical analyses of meteorites: a compilation of stony and iron meteorite analyses. Meteoritics 25, 323–337 (1990).

Kitamura Y. and Shimizu M. Oxygen isotopic anomaly and solar nebular

photochemistry *Moon and Planets, 29,* 199_202 (1983).

Kobayashi, S., Imai, H. & Yurimoto, H. New extreme ^{16}O-rich reservoir in the early solar system. *Geochem. J.* 37, 663-669 (2003).

Krot, A. N., Fegley B., J., K., L. & Palme, H. in *Protostars and Planets IV* (eds. Mannings, V., Boss, A. P. & Russell, S. S.) 1019-1054 (The University Arizona Press, Tucson, 2000).

Krot, A. N., McKeegan, K. D., Leshin, L. A., MacPherson, G. J. & Scott, E. R. D. Existence of an ^{16}O-rich gaseous reservoir in the solar nebula. *Science* 295, 1051-1054 (2002).

Krot, A. N. et al. Evolution of oxygen isotopic composition in the inner solar nebula. *Astrophys. J.* 622, 1333-1342 (2005).

Kunihiro T., Nagashima K., Takayanagi I., Nakamura J., Kosaka K. and Yurimoto H. Noise characteristics of stacked CMOS active pixel sensor for charged particles. *Nucl. Instr. and Meth. A* (2001a).

Kunihiro, T., Nagashima, K. & Yurimoto, H. Microscopic oxygen isotopic homogeneity/heterogeneity in the matrix of the Vigarano CV3 chondrite. *Geochim. Cosmochim. Acta* 69, 763-773 (2005).

Lauretta, D. S., Kremser, D. T. & Fegley, B., Jr. . The rate of iron sulfide formation in the solar nebula. *Icarus* 122, 288-315 (1996).

Lee T. A local proton irradiation model for isotopic anomalies in the solar system *Astrophys. J., 224,* 217-226 (1978).

Llorca J., Casanova I. Reaction between H2, CO, and H2S over Fe, Ni metal in the solar nebula: Experimental evidence for the formation of sulfur-bearing organic molecules and sulfides. *Earth Planet. Sci. Lett., 35,* 841-848 (2000).

Lyons, J. R. & Young, E. D. CO self-shielding as the origin of oxygen isotope anomalies in the early solar nebula. *Nature* 435, 317-320 (2005).

McSween H. Y. Alteration in CM carbonaceous chondrites inferred from modal and chemical variations in matrix. Geochim. Cosmochim. Acta 43, 1761–1770 (1979a).

McSween H. Y. Are carbonaceous chondrites primitive or processed? A review. Rev. Geophys. Space Phys. 17, 1059–1078 (1979b).

Majoube, M., Oxygen-18 and deuterium fractionation between water and steam: Journal de Chimie Physique et de Physico-chimie Biologique, 68, 1423–1971 (1971).

Matsumoto K., Yurimoto H., Kosaka K., Miyata K., Nakamura T. and Sueno S. A novel ion imager for secondary ion mass spectrometry. *IEEE Trans. Electro. Devices*

40, 82 (1993).

Marcus R. A. Mass-independent isotope effect in the earliest processed solids in the solar system: A possible chemical mechanism. *J. Chem. Phys., 121,* 8201_8211 (2004).

M.W. Chase, J. NIST-JANAF Thermochemical Tables, Fourth edition, Journal of Physical and Chemical Reference Data, Monograph 9, (Part I and Part II) (American Institute of Physics, New York, 1998).

Nagashima K., Kunihiro T., Takayanagi T., Hirata T. and Yurimoto H. Characteristics of output signal of Amplified MOS Imager. In *Proc. International Symposium on Atomic Level Characterizations for New Materials and Devises '97*, 339-342 (1997).

Nagashima K., Kunihiro T., Takayanagi I., Nakamura J., Kosaka K. and Yurimoto H. Application of active pixel sensor for charged particles to mass spectrometry. *ITE Technical Report (in Japanese)* 24(3), 13-18 (2000).

Nagashima K, Kunihiro T, Takayanagi I, Nakamura J, Kosaka K, Yurimoto H. Output characteristics of stacked CMOS-type active pixel sensor for charged particles. *Surf. interface anal.* (2001).

Nagashima, K., Krot, A. N. & Yurimoto, H. Stardust silicates from primitive meteorites. *Nature* 428, 921-924 (2004).

Navon O. and Wasserburg G. J. Self-shielding in O2-A possible explanation for oxygen isotopic anomalies in meteorites? *Earth Planet. Sci. Lett., 73,* 1_16 (1985).

Newton, J. et al. Acfer 094, a uniquely primitive carbonaceous chondrite from the Sahara. Meteoritics 30, 47–56 (1995).

Nguyen, A. N., & Zinner, E. Discovery of Ancient Silicate Stardust in a Meteorite. Science, 303, 1496 (2004).

Nittler L. R. Presolar stardust in meteorites: recent advances and scientific frontiers *Earth Planet. Sci. Lett., 209,* 259-273 (2003).

Odem R. W., Furman B. K., Evans Jr C. A., Bryson C. E., Petersen W. A. , Kelly M. A.,Wayne D. H. Quantitative image acquisition system for ion microscopybased on the resistive anode encoder. *Anal. Chem.* 55, 574-578 (1983).

Studier M.H, Hayatsu R., Anders E.,, T. Origin of organic matter in early solar system—I. Hydrocarbons. *Geochim. Cosmochim. Acta* 32, 151-173 (1968).

Takayanagi I., Nagai K., Tetsuka H., Inoue Y., Araki S., Mochimaru S., Iketaki Y., Horikawa Y., Matsumoto K. Amplified MOS Imager for Soft X-ray Imaging. *IEEE TRANSACTIONS ON ELECTRON DEVICES, VOL. 42, NO. 8,* (1995)

Takayanagi I., Nakamura J., Yurimoto H., Kunihiro T., Nagashima K., Kosaka K. CMOS image sensor for charge particle detection. *Technical Report of IEICE (in Japanese)*. 99(374), 7-12 (1999b).

Takayanagi I., Nakamura J., Yurimoto H., Fossum E.R., Kunihiro T., Nagashima K. Dark Current Reduction in Stacked-Type CMOS-APS for Charged Particle Imaging. *IEEE TRANSACTIONS ON ELECTRON DEVICES, VOL. 50, NO. 1,* (2003)

Thiemens M. H. and Heidenreich J. E. The Mass-Independent Fractionation of Oxygen: A Novel Isotope Effect and Its Possible Cosmochemical Implications *Science, 219,* 1073_1075 (1983).

Tomeoka, K. & Buseck, P. R. Indicators of aqueous alteration in CM carbonaceous chondrites: Microtextures of a layered mineral containing Fe, S, O and Ni. *Geochim. Cosmochim. Acta* 49, 2149-2163 (1985).

Trigo-Rodriguez J. M., Rubin A. E., and Wasson J. T. Nonnebular origin of dark mantles around chondrules and inclusions in CM chondrites. Geochim. Cosmochim. Acta 70, 1271–1290 (2006).

Young, E. D. & Russell, S. S. Oxygen reservoirs in the early solar nebula inferred from an Allende CAI. *Science* 282, 452-455 (1998).

Young, E. D. The hydrology of carbonaceous chondrite parent bodies and the evolution of planet progenitors. . *Phil. Tran. R. Soc. Lond. A* 359, 2095-2110 (2001).

Yurimoto, H., Ito, M. & Nagasawa, H. Oxygen isotope exchange between refractory inclusion in Allende and solar nebula gas. *Science* 282, 1874-1877 (1998).

Yurimoto H., Matsumoto K. Slid-state imager for charged particles. *Bunseki Kagaku (in Japanese)*. 45, 493-500 (1996).

Yurimoto H., Matsumoto K., Kim K., Kitajima H., Kosaka K., Hirata T. Development of solid-state two-dimensional ion imaging device and new computer control system for SIMS. In *Secondary Ion Mass Spectrometry SIMS X*, Benninghoven A., Hagenhoff B., Werner H. W. (eds). John Wiley & Sons: Chichester, 987-990 (1997).

Yurimoto, H. & Kuramoto, K. A possible scenario introducing heterogeneous oxygen isotopic distribution in proto-planetary disks. *Meteorit. Planet. Sci.* 37, A153 (2002).

Yurimoto, H., Nagashima, K. & Kunihiro, T. High precision isotope micro-imaging of materials. *Appl. Surf. Sci.* 203-204, 793-797 (2003).

Yurimoto, H. & Kuramoto, K. Molecular cloud origin for the oxygen isotope heterogeneity in the solar system. *Science* 305, 1763-1766 (2004).

Yurimoto, H. et al. in *Protostars and Planets V* (eds. Reipurth, B., Jewitt, D. & Keil, K.) 849–862 (University of Arizona Press, Tuson, 2007).

van Dishoeck E. F. and Black J. H. The photodissociation and chemistry of interstellar CO. *Astrophys. J., 334,* 771-802 (1988).

Wiza, Joseph Ladislas. Microchannel Plate Detectors. *Nuc. Instr. Meth.*, 162, 587 (1979).

Zheng Y. F. and Simon K. Oxygen isotope fractionation in hematite and magnetite : a theoretical calculation and application to geothermometry of metamorphic iron-formations. *Eur. J. Mineral.* 3, 877-886 (1991).

Zolensky M., and Browning L. CM chondrites exhibit the complete petrologic range from type 2 to 1 (abstract). Meteoritics 29, 556 (1994).